(12) INTERNATIONAL APPLICATION PUBLISHED UNDER THE PATENT COOPERATION TREATY (PCT)

(19) World Intellectual Property Organization
International Bureau

(43) International Publication Date
20 February 2003 (20.02.2003)

PCT

(10) International Publication Number
WO 03/015198 A2

(51) International Patent Classification[7]: H01M 4/50

(21) International Application Number: PCT/US02/24684

(22) International Filing Date: 2 August 2002 (02.08.2002)

(25) Filing Language: English

(26) Publication Language: English

(30) Priority Data:
60/310,622 7 August 2001 (07.08.2001) US

(71) Applicant: 3M INNOVATIVE PROPERTIES COMPANY [US/US]; 3M Center, P.O. Box 33427, Saint Paul, MN 55133-3437 (US).

(72) Inventors: DAHN, Jeffrey, R.; P.O. Box 33427, Saint Paul, MN 55133-3427 (US). LU, ZHONGHUA; P.O. Box 33427, Saint Paul, MN 55133-3427 (US).

(74) Agents: WEISS, Lucy, C. et al.; Office of Intellectual Property Counsel, Minnesota Mining and Manufacturing Company, P.O. Box 33427, St. Paul, MN 55133-3427 (US).

(81) Designated States *(national)*: AE, AG, AL, AM, AT (utility model), AT, AU, AZ, BA, BB, BG, BR, BY, BZ, CA, CH, CN, CO, CR, CU, CZ (utility model), CZ, DE (utility model), DE, DK (utility model), DK, DM, DZ, EC, EE (utility model), EE, ES, FI (utility model), FI, GB, GD, GE, GH, GM, HR, HU, ID, IL, IN, IS, JP, KE, KG, KP, KR, KZ, LC, LK, LR, LS, LT, LU, LV, MA, MD, MG, MK, MN, MW, MX, MZ, NO, NZ, OM, PH, PL, PT, RO, RU, SD, SE, SG, SI, SK (utility model), SK, SL, TJ, TM, TN, TR, TT, TZ, UA, UG, UZ, VN, YU, ZA, ZM, ZW.

(84) Designated States *(regional)*: ARIPO patent (GH, GM, KE, LS, MW, MZ, SD, SL, SZ, TZ, UG, ZM, ZW), Eurasian patent (AM, AZ, BY, KG, KZ, MD, RU, TJ, TM), European patent (AT, BE, BG, CH, CY, CZ, DE, DK, EE, ES, FI, FR, GB, GR, IE, IT, LU, MC, NL, PT, SE, SK, TR), OAPI patent (BF, BJ, CF, CG, CI, CM, GA, GN, GQ, GW, ML, MR, NE, SN, TD, TG).

Declarations under Rule 4.17:

— *as to applicant's entitlement to apply for and be granted a patent (Rule 4.17(ii)) for the following designations AE, AG, AL, AM, AT, AU, AZ, BA, BB, BG, BR, BY, BZ, CA, CH, CN, CO, CR, CU, CZ, DE, DK, DM, DZ, EC, EE, ES, FI, GB, GD, GE, GH, GM, HR, HU, ID, IL, IN, IS, JP, KE, KG, KP, KR, KZ, LC, LK, LR, LS, LT, LU, LV, MA, MD, MG, MK, MN, MW, MX, MZ, NO, NZ, OM, PH, PL, PT, RO, RU, SD, SE, SG, SI, SK, SL, TJ, TM, TN, TR, TT, TZ, UA, UG, UZ, VN, YU, ZA, ZM, ZW, ARIPO patent (GH, GM, KE, LS, MW, MZ, SD, SL, SZ, TZ, UG, ZM, ZW), Eurasian patent (AM, AZ, BY, KG, KZ, MD, RU, TJ, TM), European patent (AT, BE, BG, CH, CY, CZ, DE, DK, EE, ES, FI, FR, GB, GR, IE, IT, LU, MC, NL, PT, SE, SK, TR), OAPI patent (BF, BJ, CF, CG, CI, CM, GA, GN, GQ, GW, ML, MR, NE, SN, TD, TG)*

--- *as to the applicant's entitlement to claim the priority of the earlier application (Rule 4.17(iii)) for all designations*

Published:

— *without international search report and to be republished upon receipt of that report*

For two-letter codes and other abbreviations, refer to the "Guidance Notes on Codes and Abbreviations" appearing at the beginning of each regular issue of the PCT Gazette.

WO 03/015198 A2

(54) Title: IMPROVED CATHODE COMPOSITIONS FOR LITHIUM ION BATTERIES

(57) Abstract: A cathode composition for a lithium ion battery that contains lithium having the formula (a) $Li_y[M^1_{(1-b)}Mn_b]O_2$ or (b) $Li_y[M^1_{(1-b)}Mn_b]O_{1.5+c}$ where $0 \le y < 1$, $0 < b < 1$ and $0 < c < 0.5$ and M^1 represents one or more metal elements, with the proviso that for (a) M^1 is a metal element other than chromium. The composition is in a form of a single phase having an O3 crystal structure that does not undergo a phase transformation to a spinel crystal structure when incorporated in a lithium-ion battery and cycled for 100 full charge-discharge cycles at 30C and a final capacity of 130 mAh/g using a discharge current of 30 mA/g.

IMPROVED CATHODE COMPOSITIONS FOR LITHIUM ION BATTERIES

STATEMENT OF PRIORITY

This application claims the priority of U.S. Provisional Application No. 60/310,622 filed August 7, 2001, the contents of which are hereby incorporated by reference.

TECHNICAL FIELD

This invention relates to compositions useful as cathodes for lithium ion batteries.

BACKGROUND

Lithium-ion batteries typically include an anode, an electrolyte, and a cathode that contains lithium in the form of a lithium-transition metal oxide. Examples of lithium-transition metal oxides that have been used include lithium cobalt oxide, lithium nickel oxide, and lithium manganese oxide. None of these materials, however, exhibits an optimal combination of high initial capacity, high thermal stability, and good capacity retention after repeated charge-discharge cycling.

SUMMARY

In general, the invention features a cathode composition for a lithium ion battery that contains lithium having the formula (a) $Li_y[M^1_{(1-b)}Mn_b]O_2$ or (b) $Li_y[M^1_{(1-b)}Mn_b]O_{1.5+c}$ where $0 \leq y < 1$, $0 < b < 1$ and $0 < c < 0.5$ and M^1 represents one or more metal elements, with the proviso that for (a) M^1 is a metal element other than chromium.

The composition is in the form of a single phase having an O3 crystal structure that does not undergo a phase transformation to a spinel crystal structure when incorporated in a lithium-ion battery and cycled for 100 full charge-discharge cycles at 30°C and a final capacity of 130 mAh/g using a discharge current of 30 mA/g. The invention also features lithium-ion batteries incorporating these cathode compositions in combination with an anode and an electrolyte.

In one embodiment of (b), $b=(2-x)/3$ and $M^1_{(1-b)}$ has the formula $Li_{(1-2x)/3}M^2_x$, where $0 < x < 0.5$ and $0 < y < 1$ and M^2 represents one or more metal elements, with the proviso that the weighted average oxidation state of all M^2 is 2 when in a fully uncharged state and 4

when in a fully charged state. The resulting cathode composition has the formula $Li_y[Li_{(1-2x)/3}\ M^2_xMn_{(2-x)/3}]O_{1.5+x}$. An example of M^2 is nickel.

In a second embodiment of (a); b, $M^1_{(1-b)}$, M^2 and x are defined as in the first embodiment, with the proviso that $(1-2x) \leq y<1$ and M^2 is a metal element other than chromium. The resulting cathode composition has the formula $Li_y[Li_{(1-2x)/3}\ M^2_xMn_{(2-x)/3}]O_2$. An example of M^2 is nickel.

In a third embodiment of (b); b, $M^1_{(1-b)}$, M^2 and x are defined as in the first embodiment, with the proviso that $0<y<(1-2x)$, $0<a<(1-y)$ and M^2 is a metal element other than chromium. The resulting cathode has the formula $Li_{y+a}[Li_{(1-2x)/3}\ M^2_xMn_{(2-x)/3}]O_{1.5+x+y/2}$. An example of M^2 is nickel.

In a fourth embodiment of (b); b, $M^1_{(1-b)}$, M^2 and x are defined as in the first embodiment, with the proviso that $0<y<(1-2x)$. The resulting cathode composition has the formula

$Li_y[Li_{(1-2x)/3}\ M^2_xMn_{(2-x)/3}]O_{1.5+x+y/2}$. An example of M^2 is nickel.

In a fifth embodiment of (b) ; b=(2-2x)/3 and $M^1_{(1-b)}$ has the formula $Li_{(1-x)/3}\ M^2_x$, where $0<x<1$ and $0<y<1$ and M^2 represents one or more metal elements, with the proviso that the weighted average oxidation state of all M^2 is 3 when in a fully uncharged state and 4 when in a fully charged state. The resulting cathode composition has the formula $Li_y[Li_{(1-x)/3}\ M^2_xMn_{(2-2x)/3}]O_{1.5+x/2}$. Examples of M^2 are Co or Fe and combinations therof.

In a sixth embodiment of (b); b=(2-2x)/3 and $M^1_{(1-b)}$ has the formula $Li_{(1-x)/3}\ M^2_x$, $0<a<(1-y)$, $0<x<1$, $0<y<(1-x)$ and M^2 represents one or more metal elements, with the proviso that the weighted average oxidation state of all M^2 is 3 when in a fully uncharged state and 4 when in a fully charged state. The resulting cathode composition has the formula $Li_y[Li_{(1-x)/3}\ M^2_xMn_{(2-2x)/3}]O_{1.5+x/2}$. Examples of M^2 are Co or Fe and combinations therof.

In a seventh embodiment of (a); b, $M^1_{(1-b)}$, M^2 and x are defined as in the fifth embodiment with the proviso that $(1-x) \leq y<1$ and M^2 is a metal element other than chromium. The resulting cathode composition has the formula $Li_y[Li_{(1-x)/3}M^2_xMn_{(2-2x)/3}]O_2$. Examples of M^2 are Co or Fe and combinations thereof.

In an eighth embodiment of (b); b, $M^1_{(1-b)}$, M^2 and x are defined as in the fifth embodiment, with the proviso that $0 \leq y<(1-x)$. The resulting cathode composition has the formula

$Li_y[Li_{(1-x)/3}M^2_xMn_{(2-2x)/3}]O_{1.5+x/2+y2}$. Examples of M^2 are Co or Fe and combinations thereof.

In a ninth embodiment of (b); b=(2-2x)/3 and $M^1_{(1-b)}$ has the formula $Li_{(1-x)/3}M^2_x$, where $0<x<0.33$ and $0<y<1$ and M^2 represents one or more metal elements, with the proviso that the weighted average oxidation state of all M^2 is 3 when in a fully uncharged state and 6 when in a fully charged state. The resulting cathode composition has the formula $Li_y[Li_{(1-x)/3}M^2_xMn_{(2-2x)/3}]O_{1.5+1.5x}$. An example of M^2 is chromium.

In a tenth embodiment of (b);); b=(2-2x)/3 and $M^1_{(1-b)}$ has the formula $Li_{(1-x)/3}M^2_x$, $0<a<(1-y)$, $0<x<0.33$, $0<y<(1-3x)$, and M^2 represents one or more metal elements, with the proviso that the weighted average oxidation state of all M^2 is 3 when in a fully uncharged state and 6 when in a fully charged state. The resulting cathode composition has the formula $Li_{y+a}[Li_{(1-x)/3}M^2_xMn_{(2-2x)/3}]O_{1.5+1.5x+y/2}$. An example of M^2 is chromium.

In an eleventh embodiment of (b); b=(2-2x)/3 and $M^1_{(1-b)}$ has the formula $Li_{(1-x)/3}M^2_x$, where $0<x<0.33$ and $0<y<(1-3x)$ and M^2 represents one or more metal elements, with the proviso that the weighted average oxidation state of all M^2 is 3 when in a fully uncharged state and 6 when in a fully charged state. The resulting cathode composition has the formula $Li_y[Li_{(1-x)/3}M^2_xMn_{(2-2x)/3}]O_{1.5+1.5x+y/2}$. An example of M^2 is chromium.

The invention provides cathode compositions, and lithium-ion batteries incorporating these compositions, that exhibit high initial capacities and good capacity retention after repeated charge-discharge cycling. In addition, the cathode compositions do not evolve substantial amounts of heat during elevated temperature abuse, thereby improving battery safety.

The details of one or more embodiments of the invention are set forth in the accompanying drawings and the description below. Other features, objects, and advantages of the invention will be apparent from the description and drawings, and from the claims.

DESCRIPTION OF DRAWINGS

FIG.1a-e are plots of voltage versus capacity and capacity versus cycle number for $Li/Li[Ni_xLi_{(1/3-2x/3)}Mn_{(2/3-x/3)}]O_2$ cells with x = 1/6, 1/4, 1/3, 5/12 and ½.. The cycling was between 2.0 and 4.8 V at 5 mA/g.

FIG. 2a-e are plots of voltage versus capacity and capacity versus cycle number for Li/ $Li[Ni_xLi_{(1/3-2x/3)}Mn_{(2/3-x/3)}]O_2$ cells with x = 1/6, 1/4, 1/3, 5/12 and ½.. The cycling was between 3.0 and 4.4 V at 10 mA/g.

FIG. 3 is a plot of specific capacity versus x in $Li[Ni_xLi_{(1/3-2x/3)}Mn_{(2/3-x/3)}]O_2$ over various voltage ranges. The solid and dashed lines as indicated give expected capacities. The circles give the experimental capacity to 4.45 V, the squares give the experimental capacity of the anomalous plateau and the triangles give the experimental first charge capacity.

FIG. 4a are in-situ x-ray diffraction results for the first two charge-discharge cycles of $Li[Ni_xLi_{(1/3-2x/3)}Mn_{(2/3-x/3)}]O_2$ with x=5/12 between 3.0 and 4.4 V. FIG. 4b shows the diffraction pattern of the starting powder. The in-situ scans are synchronized with the voltage-time curve in FIG. 4c. For example, the 8th x-ray scan took place at the top of the first charge as indicated.

FIG. 5a-c are in-situ x-ray diffraction results for $Li[Ni_xLi_{(1/3-2x/3)}Mn_{(2/3-x/3)}]O_2$ with x = 5/12. FIG. 5a is the voltage-time curve; FIG. 5b are the lattice constants a and c; and FIG. 5c is the unit cell volume correlated to the voltage-time curve. The cell was cycled between 3.0 and 4.4 V

FIG. 6a-e are plots of differential capacity versus voltage for $Li/Li[Ni_xLi_{(1/3-2x/3)}Mn_{(2/3-x/3)}]O_2$ cells with x as indicated. The cells were charged and discharged between 3.0 and 4.4 V using a specific current of 10 mA/g.

FIG. 7a-c are in-situ x-ray diffraction results for $Li[Ni_xLi_{(1/3-2x/3)}Mn_{(2/3-x/3)}]O_2$ with x = 5/12. FIG. 7a is the voltage-time curve; FIG. 7b are the lattice constants a and c; and FIG. 7c is the unit cell volume correlated to the voltage-time curve. The cell was cycled between 2.0 and 4.8 V.

FIG. 8a are in-situ x-ray diffraction results for the first two charge-discharge cycles of $Li[Ni_xLi_{(1/3-2x/3)}Mn_{(2/3-x/3)}]O_2$ with x=1/6 between 2.0 and 4.8 V. FIG. 8b shows the diffraction pattern of the starting powder. The in-situ scans are synchronized with the voltage-time curve in FIG. 8c. For example, the 16th x-ray scan took place at the top of the first charge as indicated.

FIG. 9a-c are in-situ x-ray diffraction results for $Li[Ni_xLi_{(1/3-2x/3)}Mn_{(2/3-x/3)}]O_2$ with x = 1/6. FIG. 9a is the voltage-time curve; FIG. 9b are the lattice constants a and c; and FIG. 9c is

the unit cell volume correlated to the voltage-time curve. The cell was cycled between 2.0 and 4.8 V.

FIG. 10 is a Gibbs triangle for the Li - M - O ternary system with M representing $Ni_xMn_{(2/3-x/3)}$. The compositions of relevant phases are indicated.

FIG. 11 is an expanded portion of the Li - M - O Gibbs triangle of FIG. 10 showing the region of interest for the charge and discharge of $Li/Li[Ni_xLi_{(1-2x)/3}Mn_{(2-x)/3}]O_2$ cells.

FIG.12a-e are plots of differential capacity versus voltage for $Li/Li[Ni_xLi_{(1/3-2x/3)}Mn_{(2/3-x/3)}]O_2$ cells with x as indicated. The cells were charged and discharged between 2.0 and 4.8 V using a specific current of 5 mA/g.

FIG. 13 is a plot of the portion of the discharge capacity of $Li/Li[Ni_xLi_{(1-2x)/3}Mn_{(2-x)/3}]O_2$ cells (first charged to 4.8 V) due to the reduction of Mn. The points are the experimental results, the solid line is the prediction if the capacity is governed by the sites available in the Li layer (after the Ni^{4+} is reduced to Ni^{2+}) and the dashed line is the capacity available if all Mn^{4+} in the compound is reduced to Mn^{3+}.

FIG. 14a-b is an ex-situ x-ray diffraction pattern of $Li[Ni_xLi_{(1-2x)/3}Mn_{(2-x)/3}]O_2$ with x=1/3 charged to 4.8 V. The estimated stoichiometry of the sample at this potential based on oxidation state arguments (see table 1) is $[Ni_{0.33}Li_{0.113}Mn_{0.556}]O_{1.833}$. The calculated pattern is shown as the solid line. FIG. 14c and 14d show the variation of the goodness of fit (G.O.F.) and the Bragg-R factor versus the occupation of the oxygen sites.

FIG. 15a-g are plots of voltage vs. capacity for Li/Li[CrxLi(1/3-x/3)Mn(2/3-2x/3)O2 cells with x=1/6 to 1. The cycling was between 2.0 and 4.8 V at 5 mA/g.

FIG. 16a-g are plots of capacity vs. cycle number for the materials of FIG. 15a-g under the same cycling conditions.

FIG. 17a-g are plots of differential capacity vs. potential of Li/Li[CrxLi(1/3-x/3)Mn(2/3-2x/3)]O2 cells with x=1/6, ¼, 1/3, ½, 2/3, 5/6 and 1.0 between 2.0 and 4.8 V.

DETAILED DESCRIPTION

Cathode compositions have the formulae set forth in the Summary of the Invention, above. The formulae themselves, as well as the choice of particular metal elements, and combinations thereof, for M^1 and M^2, reflect certain criteria that the inventors have discovered are useful for maximizing cathode performance. First, the cathode compositions preferably adopt an O3 crystal structure featuring layers generally

arranged in the sequence lithium-oxygen-metal-oxygen-lithium. This crystal structure is retained when the cathode composition is incorporated in a lithium-ion battery and cycled for 100 full charge-discharge cycles at 30°C and a final capacity of 130 mAh/g using a discharge current of 30 mA/g, rather than transforming into a spinel-type crystal structure under these conditions. In addition, to maximize rapid diffusion in the lithium layers, and thus battery performance, it is preferred to minimize the presence of metal elements in the lithium layers. It is further preferred that at least one of the metal elements be oxidizable within the electrochemical window of the electrolyte incorporated in the battery.

The cathode compositions can be synthesized by electrochemically cycling cathode material described in Dahn, et.al. U.S.S.N. 09/845178 entitled "Improved Cathode Compositions For Lithium Ion Batteries", filed April 23, 2001. This involves synthesis by jet milling or by combining precursors of the metal elements (e.g., hydroxides, nitrates, and the like), followed by heating to generate the cathode composition. Heating is preferably conducted in air at temperatures of at least about 600°C, more preferably at least 800°C. In general, higher temperatures are preferred because they lead to materials with increased crystallinity. The ability to conduct the heating process in air is desirable because it obviates the need and associated expense of maintaining an inert atmosphere. Accordingly, the particular metal elements are selected such that they exhibit appropriate oxidation states in air at the desired synthesis temperature. Conversely, the synthesis temperature may be adjusted so that a particular metal element exists in a desired oxidation state in air at that temperature.

In general, examples of suitable metal elements for inclusion in the cathode composition include Ni, Co, Fe, Cu, Li, Zn, V, and combinations thereof. Particularly preferred cathode compositions are those having the following formulae (where weighted average oxidation state of all M^2 is 2 when in a fully uncharged state and 4 when in a fully charged state):

$Li_y[Li_{(1-2x)/3}M^2_xMn_{(2-x)/3}]O_{1.5+x}$ where $0<y<1$, $0<x<0.5$;

$Li_y[Li_{(1-2x)/3}M^2_xMn_{(2-x)/3}]O_{1.5+x+y/2}$ where $0<y<(1-2x)$ and $0<x<0.5$;

$Li_y[Li_{(1-x)/3}M^2_xMn_{(2-2x)/3}]O_2$ where $(1-2x)\leq y<1$ and $0<x<0.5$ and

$Li_{y+a}[Li_{(1-2x)/3}M^2_xMn_{(2-x)/3}]O_{1.5+x+y/2}$ where $0<a<(1-y)$, $0<y<(1-2x)$ and $0<x<0.5$.

The cathode compositions can be combined with an anode and an electrolyte to form a lithium-ion battery. Examples of suitable anodes include lithium metal, graphite,

and lithium alloy compositions, e.g., of the type described in Turner, U.S. 6,203,944 entitled "Electrode for a Lithium Battery" and Turner, WO 00/03444 entitled "Electrode Material and Compositions." The electrolyte can be liquid or solid. Examples of solid electrolytes include polymeric electrolytes such as polyethylene oxide, polytetrafluoroethylene, fluorine-containing copolymers, and combinations thereof. Examples of liquid electrolytes include ethylene carbonate, diethyl carbonate, propylene carbonate, and combinations thereof. The electrolyte is provided with a lithium electrolyte salt. Examples of suitable salts include $LiPF_6$, $LiBF_4$, and $LiClO_4$.

Specifically the electrochemical behavior of $Li/Li[Ni_xLi_{(1/3-2x/3)}Mn_{(2/3-x/3)}]O_2$ cells for x = 1/6, 1/4, 1/3, 5/12 and ½ and for Li[CrxLi(1/3-x/3)Mn(2/3-2x/3)]O2 with x = 1/6, ¼, 1/3, ½, 2/3, 5/6 and 1.0 is described herein. $Li/Li[Ni_xLi_{(1/3-2x/3)}Mn_{(2/3-x/3)}]O_2$ is derived from Li_2MnO_3 or $Li[Li_{1/3}Mn_{2/3}]O_2$ by substitution of Li^+ and Mn^{4+} by Ni^{2+} while maintaining all the remaining Mn atoms in the 4+ oxidation state. Conventional wisdom suggests that lithium can be removed from these materials only until both the Ni and Mn oxidation states reach 4^+ giving a charge capacity of 2y. We show that $Li/Li[Ni_xLi_{(1/3-2x/3)}Mn_{(2/3-x/3)}]O_2$ cells give smooth reversible voltage profiles reaching about 4.45 V when 2x Li atoms per formula unit are removed, as expected. If the cells are charged to higher voltages, surprisingly they exhibit a long plateau of length approximately equal to 1 – 2x in the range between 4.5 and 4.7 V. Subsequent to this plateau the materials can reversibly cycle over 225 mAh/g (almost one Li atom per formula unit) between 2.0 and 4.8 V. In-situ x-ray diffraction and differential capacity measurements are used to infer that irreversible loss of oxygen from the compounds with $x<1/2$ occurs during the first charge to 4.8 V. This results in oxygen deficient layered materials with stoichiometry approximately equal to $[Li_y][Ni_xLi_{(1-2x)/3}Mn_{(2-x)/3}]O_{1.5+x}$ at 4.8 V where x is approximately equal to zero. These oxygen deficient materials then reversibly react with lithium.

$Li[Ni_xLi_{(1/3-2x/3)}Mn_{(2/3-x/3)}]O_2$ is derived from Li_2MnO_3 or $Li[Li_{1/3}Mn_{2/3}]O_2$ by substitution of Li^+ and Mn^{4+} by Ni^{2+} while maintaining all the remaining Mn atoms in the 4+ oxidation state. Similar materials containing Cr^{3+} like $Li[Cr_xLi_{(1/3-x/3)}Mn_{(2/3-2x/3)}]O_2$ with x = 0.4 and containing Co^{3+}, like $Li[Co_yLi_{(1/3-y/3)}Mn_{(2/3-2y/3)}]O_2$ ($0\le y\le 1$) have been reported. In these materials the electrochemical activity during the first extraction of lithium is thought to be derived from the oxidation of Ni ($Ni^{2+} \rightarrow Ni^{4+}$, Cr ($Cr^{3+} \rightarrow Cr^{6+}$) or Co ($Co^{3+} \rightarrow Co^{4+}$). These oxidation state changes, therefore, set limits for the

maximum amount of Li that can be extracted from the compounds in a conventional intercalation process. For example, the Ni oxidation state reaches 4+ at the stoichiometry $Li_{1-2x}[Ni_xLi_{(1-2x)/3}Mn_{(2-x)/3}]O_2$, leading to an expected reversible capacity of 2x Li per formula unit.

Figure 1a-d shows the voltage-capacity curves of $Li/Li[Ni_xLi_{(1-2x)/3}Mn_{(2-x)/3}]O_2$ cells for x = 1/6, 1/4, 1/3, 5/12 and 1/2. There is a clear change in slope of the voltage profile of the first charge near 4.45 V, followed by an irreversible plateau (except for x = 1/2), whose length increases as x decreases. The capacity of the first charge between 3.0 V and 4.45 V in the sloping portion of the curve is very near to that expected when Ni reaches 4+, as we will show later below. Therefore, the origin of the long plateau is mysterious, but useful, because it leads to materials with considerably greater reversible capacity. The compositions involved in this irreversible plateau are the focus of this application.

Our first objective was to confirm that the removal of lithium from $Li[Ni_xLi_{(1-2x)/3}Mn_{(2-x)/3}]O_2$ over the range where the oxidation state of Ni is expected to be less than 4+ is a conventional intercalation process. Figures 2a-e shows the voltage versus capacity for $Li/Li[Ni_xLi_{(1/3-2x/3)}Mn_{(2/3-x/3)}]O_2$ (x = 1/6, 1/4, 1/3, 5/12, 1/2) cells between 3.0 and 4.4 V using a specific current of 10 mA/g. The capacity versus cycle number is also shown for the same cells in the right hand panels of the figures. The voltage profiles are smooth and the cells show excellent reversibility.

The solid line in figure 3 shows the capacity expected before the Ni oxidation state equals +4 plotted versus x in $Li[Ni_xLi_{(1/3-2x/3)}Mn_{(2/3-x/3)}]O_2$. This occurs at the stoichiometry $Li_{1-2x}[Ni_xLi_{(1-2x)/3}Mn_{(2-x)/3}]O_2$. The circular data points in figure 3 give the capacity to 4.45 V in figure 1, which corresponds to the capacity of the reversible cycling range in figure 2, except for the data for x = 1/2 which is taken as the full capacity shown in figure 1. There is good agreement between the prediction and the measured capacities, suggesting that Ni^{2+} is oxidized to Ni^{4+} during the portion of the charge to 4.45 V.

Figures 4a-c shows in-situ x-ray diffraction results for a $Li/Li[Ni_xLi_{(1-2x)/3}Mn_{(2-x)/3}]O_2$ cell with x = 5/12, cycled two times between 2.0 and 4.4 V. All changes to the Bragg peak positions appear to be completely reversible, as expected in an intercalation process. Figures 5a-c shows the lattice constants and the unit cell volume correlated to the voltage profile. Within the error of the experiment, the changes to the lattice constants and

the unit cell volume appear to be reversible as lithium is removed from and added to the compound.

Figures 6a-e shows the differential capacity versus voltage for the $Li/Li[Ni_xLi_{(1-2x)/3}Mn_{(2-x)/3}]O_2$ cells cycled between 3.0 and 4.4 V. Apart from small differences between the first charge cycle and later cycles thought to be caused by the impedance of the uncycled Li electrode in the freshly assembled cells, the differential capacity is perfectly repeatable for numerous cycles, suggesting a stable intercalation process for all these materials.

Figures 1a-e clearly shows that there is excess capacity available in these samples above 4.45 V which occurs as a plateau between 4.5 and 4.7 V during the first charge cycle. The length of the plateau capacity is plotted versus x in $Li[Ni_xLi_{(1/3-2x/3)}Mn_{(2/3-x/3)}]O_2$ as the squares in figure 3. The plateau capacity decreases smoothly with x. If the plateau occurs once the Ni oxidation state reaches 4+, or at the stoichiometry $Li_{1-2x}[Ni_xLi_{(1-2x)/3}Mn_{(2-x)/3}]O_2$, then the plateau should have a length of 1 - 2x per formula unit, if all Li atoms can be removed from the Li layers and provided that Li atoms cannot be extracted from the predominantly transition metal layer. This prediction is given as the long dashed line in figure 3 and agrees well with the square data points which are the experimental plateau capacities from figure 1 Finally, the total capacity of the first charge of the cells described by figure 1 is given as the triangles in figure 3, and compared to the capacity expected if all the Li atoms could be extracted from the Li layers. The agreement is quite good.

The results in figures 1-6 suggest that when the Ni oxidation state is below 4+, the compounds show reversible cycling in an intercalation process. Once the Ni oxidation state reaches 4+ (near 4.45 V), it appears that further Li can be extracted, up to the limit when all the Li has been extracted from the Li layers. There are some questions that must be answered, however. First, what happens to the transition metal oxidation states along the plateau? Second, why is the subsequent cycling after the cells have first been charged to 4.8 V so different than the initial charge (see figure 1)? Third, is it true that lithium is being extracted during the plateau, as we hypothesize? To address these questions, further in-situ XRD experiments were made.

Figures 7a-c show analyzed in-situ x-ray diffraction results for a $Li/Li[Ni_xLi_{(1-2x)/3}Mn_{(2-x)/3}]O_2$ cell with x = 5/12, cycled two times between 2.0 and 4.8 V. The lattice

constant and the unit cell volume changes are correlated to the voltage profile. Near 4.8 V, the c-axis begins to decrease rapidly, consistent with the behaviour observed (for example in $LiCoO_2$) when the last lithium atoms are removed from the lithium layers. In addition, during the plateau near 4.6 V, the a-axis remains almost constant, while the c-axis is changing. The plateau cannot correspond entirely to a parasitic side reaction involving the electrolyte, because clearly the lithium content of the material is changing. Both the clear plateau near 4.6 V and the region of constant a-axis are not observed during the second charge. Some irreversible change has occurred in the electrode during its charge to 4.8V.

In order to observe these changes more clearly, we carried out the same experiments on the sample with x = 1/6, where the plateau is very pronounced. Figures 8a-c show the raw in-situ XRD results and figures 9a-c show the lattice constants and unit cell volume correlated to the cell voltage profile. Both figures 8 and 9 clearly show that the structure of the material, as evidenced by the diffraction pattern and the lattice constants, in the discharged state (53 hours) is different from the virgin sample. In particular, the unit cell volume (Figure 9c) is much larger than in the original material. Figure 9b also shows that the a-axis does not change significantly during the plateau in the first charge between 4.5 and 4.7 V, even while the c-axis decreases rapidly. The rapid decrease in the c-axis near 4.8 V suggests again that most of the Li has been extracted from between the Li layers.

The results in figures 7, 8 and 9 suggest several things. First, the rapid decrease in the c-axis near 4.8 V suggests that most of the Li is being removed from the Li layers, consistent with the cell capacities, as shown in figure 3. The a-axis decreases smoothly with lithium content during the first charge until the anomalous plateau is reached in both figures 7 and 9. The a-axis presumably decreases because the Ni^{4+} formed during charge is smaller than Ni^{2+}. Once the plateau is reached, the a-axis remains approximately constant, suggesting that the transition metal oxidation states are not changing during the plateau. If the transition metal oxidation states do not change, then the charge removed must come from the oxygen atoms and therefore the removal of lithium must be accompanied by the expulsion of oxygen from the structure along this plateau. This expelled oxygen may react with the cell electrolyte, and may be responsible for clear

correlation between the length of the anomalous plateau in figure 1 and the irreversible capacity for the samples with x = 1/6, 1/3, 1/4 and 5/12.

The simultaneous expulsion of both lithium and oxygen from the compound during the plateau is surprising. Support for this can be found, however, in a careful study of the voltage profiles in figure 1 and a further examination of the in-situ x-ray diffraction results in figures 7 and 9. It is also useful to first consider the stoichiometry of the materials at 4.8 V.

Figure 10 shows the Gibbs triangle of the ternary Li - M - O system where we have abbreviated $Ni_xMn_{(2-x)/3}$ by M, where x is set by the nickel quantity in $Li[Ni_xLi_{(1/3-2x/3)}Mn_{(2/3-x/3)}]O_2$. The compositions of relevant phases in the triangle are given. The solid solution series $Li[Ni_xLi_{(1/3-2x/3)}Mn_{(2/3-x/3)}]O_2$ ($0 < x < 0.5$) is found on the line joining $Li[Li_{1/3}M_{2/3}]O_2$ and $LiMO_2$. The line joining $Li[Li_{1/3}M_{2/3}]O_2$ and MO_2 represents a line of constant transition metal oxidation state equal to 4+. Figure 11 shows an expanded view of the Gibbs triangle in the region of interest to describe the charge of a $Li/Li[Ni_xLi_{(1/3-2x/3)}Mn_{(2/3-x/3)}]O_2$ cell.

The path of the stoichiometry of the electrode particles is traced by the heavy solid line in figure 11 which is illustrated for the case x = 1/6. The electrode in the freshly assembled cell begins at the point of intersection between the heavy solid line and the line joining $Li[Li_{1/3}M_{2/3}]O_2$ and $LiMO_2$. During the charge to 4.45 V, the electrode composition moves to the point "A". This corresponds to the stoichiometry $Li_{1-2x}[Ni_xLi_{(1-2x)/3}Mn_{(2-x)/3}]O_2$ for x = 1/6 as given in table 1. Next, we assume that the overall stoichiometry of the electrode material continues to move on a straight line between "A" and "D", into a two-phase region between oxygen gas and a solid with transition metals in oxidation state 4+. Thus, the solid portion of the electrode moves from "A" to "B". At the point "B", we assume that the transition metals are in oxidation state 4+ and that all Li is removed from the Li layers, leading to the stoichiometry $[\ ][Ni_xLi_{(1-2x)/3}Mn_{(2-x)/3}]O_{1.5+x}$ at the point "B" as shown in figure 11 and table 1. Now, during the next discharge cycle, we assume that lithium is simply added to this oxygen deficient layered phase, until the Li layers are filled again, corresponding to the path from "B" to "C" in figure 11. The point "C" in figure 11 has the stoichiometry $Li[Ni_xLi_{(1-2x)/3}Mn_{(2-x)/3}]O_{1.5+x}$ (for x = 1/6) as given in table 1. Subsequent cycling occurs between "B" and "C".

The scenario described by the heavy line in figure 11 predicts that the first charge should be different from subsequent cycles, as observed in figure 1. Figure 12 reinforces this point by showing that the differential capacity versus voltage of the first charge to 4.8 V is different than the next cycles for the cells described by figure 1. The subsequent cycles are very reversible, as predicted by the line from "B" to "C" in figure 11.

If the oxygen content of the solid portion of the electrode is reduced along the line from "A" to "B", then there will be a point during the subsequent discharge where the reduction of Mn must occur. If we assume that Ni^{4+} is first completely reduced to Ni^{2+} and then Mn^{4+} is reduced, we can predict the point where Mn reduction should occur. The stoichiometry where Mn reduction first occurs based on this assumption is $Li_{2x}[Ni_xLi_{(1-2x)/3}Mn_{(2-x)/3}]O_{1.5+x}$ as given in table 1.

Table 1. Stoichiometry of $Li[Ni_xLi_{(1-2x)/3}Mn_{(2-x)/3}]O_2$ starting material assuming all Ni and Mn are in the +4 oxidation state (2nd column); the stoichiometry reached when all Ni has been oxidized to Ni^{4+} near 4.45 V (3rd column); the stoichiometry reached when all Li is removed from the Li layer (4.8 V), assuming Ni and Mn cannot be oxidized beyond 4+ and oxygen loss can occur (4th column); the stoichiometry reached when all Ni has been reduced to Ni^{2+} during discharge and Mn begins to be reduced (near 3.5 V) (2nd column of lower table); the stoichiometry reached at 2.5 V, assuming all sites in the Li layer can be re-filled (3rd column of lower table); the Mn oxidation state reached at 2.5 V, assuming all Ni is Ni^{2+} (4th column of lower table); and the unit cell volume measured from in-situ XRD experiments at various states of charge for two of the samples.

X	Initial Stoichiometry	Stoichiometry at 4.45 V	Stoichiometry at 4.8 V
X	$Li[Ni_xLi_{(1-2x)/3}Mn_{(2-x)/3}]O_2$	$Li_{1-2x}[Ni_xLi_{(1-2x)/3}Mn_{(2-x)/3}]O_2$	$[Ni_xLi_{(1-2x)/3}Mn_{(2-x)/3}]O_{1.5+x}$
0.167	$Li[Ni_{0.167}Li_{0.222}Mn_{0.611}]O_2$	$Li_{0.667}[Ni_{0.167}Li_{0.222}Mn_{0.611}]O_2$	$[Ni_{0.167}Li_{0.222}Mn_{0.611}]O_{1.667}$
0.25	$Li[Ni_{0.25}Li_{0.167}Mn_{0.583}]O_2$	$Li_{0.5}[Ni_{0.25}Li_{0.167}Mn_{0.583}]O_2$	$[Ni_{0.25}Li_{0.167}Mn_{0.583}]O_{1.75}$
0.333	$Li[Ni_{0.33}Li_{0.113}Mn_{0.556}]O_2$	$Li_{0.33}[Ni_{0.33}Li_{0.113}Mn_{0.556}]O_2$	$[Ni_{0.33}Li_{0.113}Mn_{0.556}]O_{1.833}$
0.416	$Li[Ni_{0.416}Li_{0.056}Mn_{.528}]O_2$	$Li_{0.168}[Ni_{0.416}Li_{0.056}Mn_{.528}]O_2$	$[Ni_{0.416}Li_{0.056}Mn_{.528}]O_{1.916}$
0.5	$Li[Ni_{0.5}Mn_{0.5}]O_2$		$[Ni_{0.5}Mn_{0.5}]O_2$

X	Stoichiometry when Mn begins to be reducedduring discharge	Stoichiometry at 2.5 V	Mn oxidation state at 2.5 V	Initial unit cell volume ($Å^3$)	Unit cell volume ($Å^3$) at 4.8 V	Unit cell volume ($Å^3$) at 2.5 V
X	$Li_{2x}[Ni_xLi_{(1-2x)/3}Mn_{(2-x)/3}]O_{1.5+x}$	$Li[Ni_xLi_{(1-2x)/3}Mn_{(2-x)/3}]O_{1.5+x}$	(5+2x)/(2-x)			
0.167	$Li_{0.33}[Ni_{0.167}Li_{0.222}Mn_{0.611}]O_{1.667}$	$Li[Ni_{0.167}Li_{0.222}Mn_{0.611}]O_{1.667}$	2.91	100.7	98.2	103.0
0.25	$Li_{0.5}[Ni_{0.25}Li_{0.167}Mn_{0.583}]O_{1.75}$	$Li[Ni_{0.25}Li_{0.167}Mn_{0.583}]O_{1.75}$	3.14			
0.333	$Li_{0.66}[Ni_{0.33}Li_{0.113}Mn_{0.556}]O_{1.833}$	$Li[Ni_{0.33}Li_{0.113}Mn_{0.556}]O_{1.833}$	3.40			
0.416	$Li_{0.83}[Ni_{0.416}Li_{0.056}Mn_{.528}]O_{1.916}$	$Li[Ni_{0.416}Li_{0.056}Mn_{.528}]O_{1.916}$	3.68	102.5	98.8	103.0
0.5	$Li[Ni_{0.5}Mn_{0.5}]O_2$	$Li[Ni_{0.5}Mn_{0.5}]O_2$	4.0			

A critical comparison of the differential capacities in figures 6a-e (only Ni being oxidized and reduced) and 12a-e (both Ni and Mn being oxidized and reduced) suggests that the capacity below about 3.5 V during discharge must be due to the reduction of Mn. The capacity attributable to Mn reduction based on this model is 1 - 2x per formula unit. This prediction is shown as the solid line in figure 13 and is compared to the experimental discharge capacity below 3.5 V. The agreement is very good for the samples with $x \geq 1/3$. We take this qualitative agreement as conclusive evidence for the extraction of oxygen from the sample along the plateau for otherwise Mn reduction would not be required. A further consideration is that it may not be possible to reduce Mn beyond Mn^{3+} at these potentials, even if the Li layer is not filled. The dashed line in figure 13 shows the capacity available based on the reduction of all the Mn^{4+} to Mn^{3+}. Notice that the solid and dashed lines cross near $x = 0.2$ which is close to the point where the experimental points appear to deviate from the solid line. The samples with $x < 1/3$ do not agree well with either prediction. However these show substantial irreversible capacity which may be related to the large amounts of oxygen removed along the plateau. When so much oxygen is removed, it may be that substantial motion of the transition metals to the lithium layer may occur, leading to poor lithium diffusion and large irreversible capacity.

A comparison of the c-axis variation with lithium content in figures 7b (for $x = 5/12$) and 9b (for $x = 1/6$) is instructive. When $x = 5/12$, the c-axis first increases as lithium is extracted from the host and only when most of the lithium is extracted does the

c-axis fall rapidly. This is consistent with the behaviour observed for layered compounds like $LiCoO_2$. By contrast, the sample with x = 1/6, (figure 9c) shows a relatively smooth variation of the c-axis with lithium content after crossing the anomalous plateau. This may suggest a transfer of some transition metals into the lithium layer. These heavy cations in the Li layer could be the cause of the large irreversible capacity observed for this sample since they would make it difficult to insert lithium into every available site due to slow diffusion.

Table 1 gives the expected Mn oxidation state at the point "C" in figure 11. Samples with smaller x in $Li[Ni_xLi_{(1/3-2x/3)}Mn_{(2/3-x/3)}]O_2$ have smaller Mn oxidation states at point "C" than do those with larger x. Since Mn^{2+} and Mn^{3+} are larger than Mn^{4+}, we expect samples at the point "C" in figure 11, to have larger unit cell volume than the original $Li[Ni_xLi_{(1/3-2x/3)}Mn_{(2/3-x/3)}]O_2$ starting materials. This is shown to be the case for both the x = 1/6 and x = 5/12 materials in table 1. The increase in unit cell volume is largest for the sample with x = 1/6 because it has more reduced Mn than the sample with x = 5/12.

The results above strongly suggest that oxygen loss from the samples occurs during the plateau at 4.5 V. In order to confirm this, ex-situ x-ray diffraction studies of electrodes with x = 1/6, 1/3 and 5/12 charged to 4.8 V were made. Figures 14a-d show the diffraction pattern of the sample with x = 1/3 and the best-fit to experiment calculated as described below. The structural model used to calculate the diffraction pattern in figure assumed that the sample retained the O3 structure. We assumed that the lithium layers were empty of lithium, but that an amount of Ni, equal to that found on the Li layers in the original Rietveld refinement of the $Li[Ni_xLi_{(1/3-2x/3)}Mn_{(2/3-x/3)}]O_2$ starting material, remained. The occupation of the Li, Ni and Mn atoms in the transition metal layer were fixed at the occupations originally found in the starting material. The occupation of the oxygen sites was allowed to vary and the best fit was found for an oxygen occupation of 1.813, which agrees well with that expected as indicated in table 1. This assumes random loss of oxygen from the oxygen sites, creating vacancies. Figures 14c and 14d show the variation of the goodness of fit and the Bragg R-factor with the occupation of the oxygen sites. This clearly indicates that oxygen loss from the compound has occurred.

Table 2 gives the results of the Rietveld refinement of the charged electrodes. The obtained oxygen stoichiometry is compared to the predicted oxygen stoichiometry at 4.8 V

given in table 1 based on oxidation state arguments. The agreement between predicted and measured oxygen stoichiometries appears to be very good and is evidence that the charged materials are oxygen deficient.

TABLE 2 - Results of ex-situ x-ray diffraction analysis of the samples charged to 4.8 V, showing oxygen loss.

X	Refined Parameters
x=1/6	a=2.8437±0.0006Å c=14.01306±0.0089Å n(O)= 1.73±0.03 expected n(O), based on table 1 = 1.667 z(O)= 0.2397±0.0005 R_{wp}=14.54%, R_B=5.4%
x=1/3	a=2.8493±0.0004Å c=14.2288±0.0041Å n(O)= 1.813±0.016 expected n(O), based on table 1 = 1.833 z(O)= 0.2381±0.0003 R_{wp}=9.13%, R_B=2.7%
x=5/12	a=2.8478±0.0003Å c=14.1958±0.0030Å n(O)= 1.875±0.011 expected n(O), based on table 1 = 1.916 z(O)= 0.2347±0.0002 R_{wp}=7.8%, R_B=3.8%

The experimental evidence is consistent with the simultaneous extraction of both Li and O atoms along the plateau above 4.5 V during the first charge. The extraction is done in a way to keep the transition metal oxidation state fixed at 4, therefore it is as if Li_2O is being removed from the compound during this plateau.

Objects and advantages of this invention are further illustrated by the following examples, but the particular materials and amounts thereof recited in these examples, as well as other conditions and details, should not be construed to unduly limit this invention. Parts and percentages are by weight unless otherwise indicated.

EXAMPLES

Examples 1-7

$LiOH{\cdot}H_2O$(98%+, Aldrich), $Ni(NO_3)_2{\cdot}6H_2O$ (98%+, Fluka) and $Mn(NO_3)_2{\cdot}6H_2O$ (97%+, Fluka) were used as the starting materials. The samples $Li[Ni_xLi_{(1/3-2x/3)}Mn_{(2/3-x/3)}]O_2$ (0=0.0, 1/12, 1/6, ¼, 1/3, 5/12, and 1/2) were prepared by the "mixed hydroxide" method as described in Z. Lu and J.R. Dahn, J. Electrochem. Soc. 148, A237 (2001).

A 50 ml aqueous solution of the transition metal nitrates was slowly dripped (1 to 2 hours) into 400 ml of a stirred solution of LiOH using a buret. This causes the precipitation of $M(OH)_2$ (M = Mn, Ni) with what we hope is a homogeneous cation distribution. The buret was washed three times to make sure that all the transition metal nitrates were added to the LiOH solution. The precipitate was filtered out and washed twice with additional distilled water to remove the residual Li salts (LiOH and the formed $LiNO_3$). The precipitate was dried in air at 180°C overnight. The dried precipitate was mixed with the stoichiometric amount of $Li(OH){\cdot}H_2O$ and ground in an automatic grinder. Pellets about 5 mm thick were then pressed. The pellets were heated in air at 480°C for 3 hrs. Tongs were used to remove the pellets from the oven and sandwich them between two copper plates in order to quench the pellets to room temperature. The pellets were ground and new pellets made. The new pellets were heated in air at 900°C for another 3 hrs and quenched to room temperature in the same way. The samples described here are the same ones reported in USSN 09/845178.

Example 8

$CH_3CO_2Li{\cdot}2H_2O$ (98%, Aldrich), $Cr(NO_3)_3{\cdot}9H_2O$ (99%, Aldrich) and $(CH_3CO_2)2Mn{\cdot}4H_2O$ (99%+, Aldrich) were used as the starting materials. The samples $Li[Cr_xLi_{(1/3-x/3)}Mn_{(2/3-2x/3)}]O_2$ (0=1/6, ¼, 1/3, ½, 2/3, 5/6, and 1.0) were prepared by the "Sol-gel" method. Stoichiometric amounts of $CH_3CO_2Li{\cdot}2H_2O$, $Cr(NO_3)_3{\cdot}9H_2O$ and

$(CH_3CO_2)2Mn{\cdot}4H_2O$ were dissolved in about 100 ml distilled water in a 500 ml beaker while stirring. The pH of the solution was adjusted to about 10 by adding NH_4OH solution and precipitation occurred. Then the beaker was placed on a hot-plate to evaporate the water slowly while stirring. After most of the water had evaporated, the beaker was put in a muffle oven and dried in air at 130°C overnight. The dried precipitate was ground in an automatic grinder and heated in air at 480°C for 12 hrs. After cooling to room temperature, the heated powder was ground in an automatic grinder again and pellets about 5 mm thick were pressed. The pellets were heated in an argon stream at 900°C for 3 hours using a Lindberg tube furnace. The oven was heated to 900°C at a rate of 600°C/hr. After dwelling at 900°C for 3 hours, the oven was cooled to room temperature at a rate of 600°C/hr. Before heating, argon was purged through the tube oven for about 3 hrs to remove residual oxygen from the tube.

X-RAY DIFFRACTION

X-ray diffraction was carried out using a Siemens D500 diffractometer equipped with a Cu target X-ray tube and a diffracted beam monochromator. Profile refinement of the data for the powder samples was made using Hill and Howard's version of the Rietveld Program Rietica as described in Rietica v1.62, window version of LHPM, R.J. Hill and C.J. Howard, J. Appl. Crystallogr. 18, 173 (1985); D.B. Wiles and R.A. Young, J. Appl. Crystallogr.14, 149 (1981).

The materials are single phase and adopt the α-$NaFeO_2$ structure (space group R-3M, #166). In-situ x-ray diffraction measurements were made using the same diffractometer and lattice constants were determined by least squares refinements to the positions of at least 7 Bragg peaks. Rietveld profile refinement was not performed on in-situ x-ray diffraction results.

ELECTRODE PREPARATION AND TESTING

"Bellcore-type" electrodes were prepared for the electrochemical tests. Z grams of the sample is mixed with ca. 0.1Z (by weight) super S carbon black and 0.25Z Kynar 2801 (PVdF-HFP)(Elf-Atochem). This mixture was added to 3.1Z acetone and 0.4Z dibutyl phthalate (DBP, Aldrich) to dissolve the polymer.

After several hours of stirring and shaking, the slurry was then spread on a glass plate using a notch bar spreader to obtain an even thickness of 0.66 mm. When the acetone evaporated, the dry films were peeled off the plate and punched into circular disks with a diameter of 12 mm. The punched electrode was washed several times in anhydrous diethyl ether to remove the DBP. The washed electrode was dried at 90°C in air overnight before use. Using the above positive electrodes, 2325 type coin-cells (23 mm diameter, 2.5 mm thick) were assembled in an argon glove-box (water < 5 ppm, O_2 < 5 ppm) with lithium as the anode, Celgard 2502 membrane as the separator and 1M $LiPF_6$ in 33 vol% ethylene carbonate (EC) + 67 vol% diethyl carbonate (DEC) (Mitsubishi Chemical) as the electrolyte. Usually, the cathode mass was around 20 mg. The cells were tested using constant charge and discharge currents between the desired potential limits.

In-situ x-ray diffraction measurements were made in the same coin-type cells, except the can of the cell had a circular hole that was replaced by a beryllium window as described in M.N. Richard, I. Koetschau and J. R. Dahn, J. Electrochem. Soc., 144, 554 (1997). The cathode electrode was facing the beryllium, so that diffraction patterns with minimal contamination from cell hardware could be obtained. Cells were charged and discharged using constant currents and x-ray diffraction scans were collected sequentially.

In order to examine the crystal structure of $Li[Ni_xLi_{(1/3-2x/3)}Mn_{(2/3-x/3)}]O_2$ after the long charge plateau at 4.5 V, electrochemical cells were prepared for ex-situ diffraction studies. Cells using electrodes of materials with x = 1/6, 1/3 and 5/12 were charged to 4.8 V and stabilized there. After the cell current decayed to below 5 mA/g the cells were disassembled and the positive electrode recovered. The electrode was washed with EC-DEC (33%:67%) solvent to remove the dissolved salt. The electrode powder was placed on a zero background holder (510-cut Si) and a diffraction pattern was recorded. Rietveld refinement was then used to obtain the structural parameters of the sample.

Figures 15a-g and figures 16a-g show the charge-discharge curves and capacity retention versus cycle number of Li/Li[CrxLi(1/3-x/3)Mn(2/3-2x/3)]O2 cells cycled between 2.0 and 4.8 V using a specific current of 5 mA/g at 30oC. Figures 15a-g shows that the first charge profiles are quite different from the following ones and that the irreversible capacity losses are between 75 mAh/g and 150 mAh/g. Figures 16a-g shows that the delivered reversible capacity gradually decreases from about 260 mAh/g to almost 0 mAh/g as the Cr content increases from 1/6 to 1. For Li[CrxLi(1/3-x/3)Mn(2/3-

2x/3)]O2 with x = 1/6, ¼, 1/3, ½, 2/3, 5/6 and 1.0, the Cr is believed to be in 3+ oxidation state and the Mn in the 4+ oxidation state. Since Mn4+ can not be oxidized beyond the 4+ oxidation state in these experiments, the Mn4+ is assumed not to take part in the redox reaction. It has been reported that the Cr3+ in Li[Li0.2Cr0.4Mn0.4]O2 is oxidized into Cr6+ when the lithium is extracted from its structure, and simultaneously, Cr moves from the octahedral site to a neighboring tetrahedral site.

For Li[CrxLi(1/3-x/3)Mn(2/3-2x/3)]O2 with x=1/6 and ¼, the expected capacities due to the redox reaction on Cr are smaller than the first charge capacity up to 4.8 V. Like Li[NixLi1/3-2x/3Mn2/3-x/3]O2 (0<x<1/2), Li[CrxLi(1/3-x/3)Mn(2/3-2x/3)]O2 with x=1/6 and ¼ must lose some amount of oxygen during the first charge process. Figures 17a-g show the differential capacity vs. potential of Li/Li[CrxLi(1/3-x/3)Mn(2/3-2x/3)]O2 cells with x=1/6, ¼, 1/3, ½, 2/3, 5/6 and 1.0 between 2.0 and 4.8 V. Figure 17 shows that the first charge is quite different from the following ones. The features (marked with the dashed circle) during the first charge become more pronounced as the Cr content, x increases. These changes may be related to the movement of Cr during the first extraction of Li. The peak in figure 17 marked with the solid circle near 4.5 V during the first charge is due to oxygen loss. Just as in the case of Li/Li[NixLi1/3-2x/3Mn2/3-x/3]O2 (0<x<1/2) cells, this peak in dQ/dV appears as a plateau in the voltage profile of the first charge shown in figure 15. For Li/Li[CrxLi(1/3-x/3)Mn(2/3-2x/3)]O2 cells, the plateau is not as flat, and hence easy to observe, as it is for Li/Li[NixLi1/3-2x/3Mn2/3-x/3]O2 (0<x<1/2) cells.

The peak near 4.5 V in figures 17a-g becomes weaker as the Cr content increases from 1/6 to ½. This is because more Cr is available for the redox reaction. Oxygen loss should not be required for samples with x<1/3 in order to remove all the Li from the Li layer, and figures 17a-g show that the 4.5 V peak is almost gone for the x = 1/3 sample. Furthermore, figure 17a-g show that Li/Li[CrxLi(1/3-x/3)Mn(2/3-2x/3)]O2 cells with x=1/6 display extra capacity between 2.0 and 3.1 V after losing oxygen during the first charge to 4.8 V. This extra capacity is attributed to the reduction of some Mn4+ to Mn3+ -- the same behavior as observed in Li/Li[NixLi1/3-2x/3Mn2/3-x/3]O2 (1/6<x<1/3) cells.

The invention has been described with reference to specific and preferred embodiments and techniques. However, other embodiments of this invention will be apparent to those skilled in the art upon consideration of this specification or from practice of the invention disclosed herein. Various omissions, modifications, and changes to the principles and embodiments described herein may be made by one skilled in the art without departing from the true scope and spirit of the invention which is indicated by the following claims.

WHAT IS CLAIMED IS:

1. A cathode composition for a lithium ion battery having the formula (a) $Li_y[M^1_{(1-b)}Mn_b]O_2$ or (b) $Li_x[M^1_{(1-b)}Mn_b]O_{1.5+c}$ where $0 \leq y < 1$, $0 < b < 1$ and $0 < c < 0.5$ and M^1 represents one or more metal elements, with the proviso that for (a) M^1 is a metal element other than chromium;

said composition characterized as being in the form of a single phase having an O3 crystal structure that does not undergo a phase transformation to a spinel crystal structure when incorporated in a lithium-ion battery and cycled for 100 full charge-discharge cycles at 30C and a final capacity of 130 mAh/g using a discharge current of 30 mA/g.

2. A cathode composition for a lithium-ion battery having the formula $Li_y[Li_{(1-2x)/3}M^2_xMn_{(2-x)/3}]O_{1.5+x}$ where $0 < y < 1$, $0 < x < 0.5$ and M^2 represents one or more metal elements, with the proviso that the weighted average oxidation state of all M^2 is 2 when in a fully uncharged state and 4 when in a fully charged state.

3. A cathode composition for a lithium-ion battery having the formula $Li_{y+a}[Li_{(1-2x)/3}M^2_xMn_{(2-x)/3}]O_{1.5+x+y/2}$ where $0 < a < (1-y)$, $0 < y < (1-2x)$ and $0 < x < 0.5$ and M^2 represents one or more metal elements, with the proviso that the weighted average oxidation state of all M^2 is 2 when in a fully uncharged state and 4 when in a fully charged state.

4. A cathode composition for a lithium ion battery having the formula $Liy[Li_{(1-2x)/3}M^2_xMn_{(2-x)/3}]O_2$ where $(1-2x) \leq y < 1$ and $0 < x < 0.5$ and M represents one or more metal elements, with the proviso that M^2 is a metal element other than chromium and that the weighted average oxidation state of all M^2
is 2 when in a fully uncharged state and 4 when in a fully charged state.

5. A cathode composition for a lithium ion battery having the formula $Li_y[Li_{(1-2x)/3}M^2_xMn_{(2-x)/3}]O_{1.5+x+y/2}$ where $0 < y < (1-2x)$ and $0 < x < 0.5$ and M^2 represents one or more metal elements, with the proviso that the weighted average oxidation state of all M^2 is 2 when in a fully uncharged state and 4 when in a fully charged state.

6. A cathode composition for a lithium-ion battery having the formula $Li_y[Li_{(1-x)/3}M^2_xMn_{(2-2x)/3}]O_{1.5+x/2}$ where $0<y<1$ and $0<x<1$ and M^2 represents one or more metal elements, with the proviso that the weighted average oxidation state of all M is 3 when in a fully uncharged state and 4 when in a fully charged state.

7. A cathode composition for a lithium-ion battery having the formula $Li_{y+a}[Li_{(1-x)/3}M^2_xMn_{(2-2x)/3}]O_{1.5+x/2+y/2}$ where $0<a<(1-y)$, $0<y<(1-x)$ and $0<x<1$ and M^2 represents one or more metal elements, with the proviso that the weighted average oxidation state of all M^2 is 3 when in a fully uncharged state and 4 when in a fully charged state.

8. A cathode composition for a lithium ion battery having the formula $Li_y[Li_{(1-x)/3}M^2_xMn_{(2-2x)/3}]O_2$ where $(1-x)\leq y<1$ and $0<x<1$ and M^2 represents one or more metal elements, with the proviso that M^2 is a metal element other than chromium and that the weighted average oxidation state of all M^2
is 3 when in a fully uncharged state and 4 when in a fully charged state.

9. A cathode composition for a lithium-ion battery having the formula $Li_y[Li_{(1-x)/3}M^2_xMn_{(2-2x)/3}]O_{1.5+x/2+y2}$ where $0<y<(1-x)$ and $0<x<1$ and M^2 represents one or more metal elements, with the proviso that the weighted average oxidation state of all M^2 is 3 when in a fully uncharged state and 4 when in a fully charged state.

10. A cathode composition for a lithium-ion battery having the formula $Li_y[Li_{(1-x)/3}M^2_xMn_{(2-2x)/3}]O_{1.5+1.5x}$ where $0<y<1$ and $0<x<0.33$ and M^2 represents one or more metal elements, with the proviso that the weighted average oxidation state of all M^2 is 3 when in a fully uncharged state and 6 when in a fully charged state.

11. A cathode composition for a lithium-ion battery having the formula $Li_{y+a}[Li_{(1-x)/3}M^2_xMn_{(2-2x)/3}]O_{1.5+1.5x+y/2}$ where $0<a<(1-y)$, $0<y<(1-3x)$ and $0<x<0.33$ and M^2 represents one or more metal elements, with the proviso that the weighted average

oxidation state of all M^2 is 3 when in a fully uncharged state and 6 when in a fully charged state.

12. A cathode composition for a lithium-ion battery having the formula $Li_y[Li_{(1-x)/3}M^2_xMn_{(2-2x)/3}]O_{1.5+1.5x+y/2}$ where $0<y<(1-3x)$ and $0<x<0.33$ and M^2 represents one or more metal elements, with the proviso that the weighted average oxidation state of all M^2 is 3 when in a fully uncharged state and 4 when in a fully charged state.

13. A lithium-ion battery comprising:

(a) an anode;

(b) a cathode; and

(c) an electrolyte separating said anode and said cathode,

said cathode comprising the cathode composition of any one of claims 1, 2, 4, 6, 8, 11, 13, 15, 17, 20, 22, and 24.

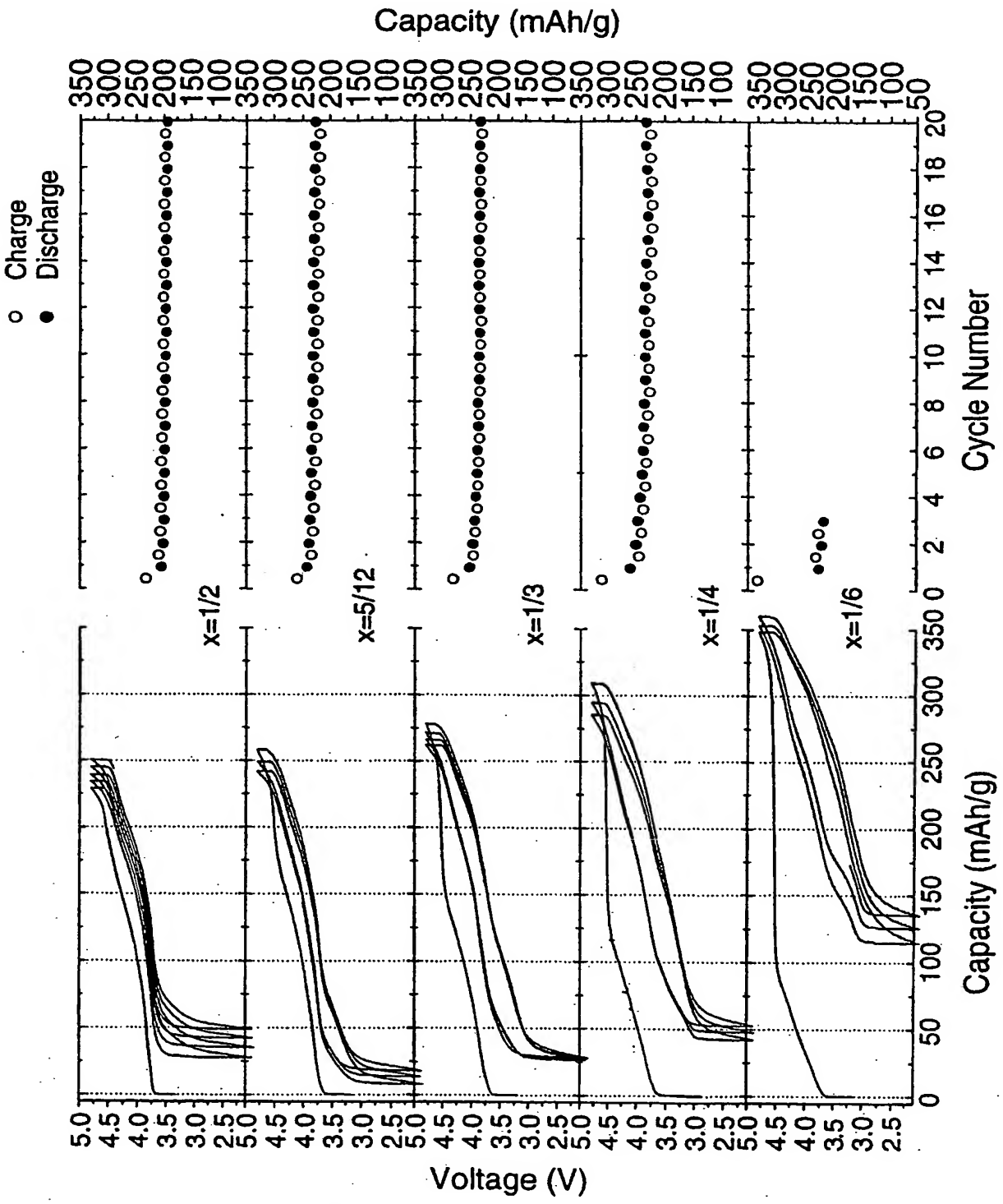

Fig. 1a

Fig. 1b

Fig. 1c

Fig. 1d

Fig. 1e

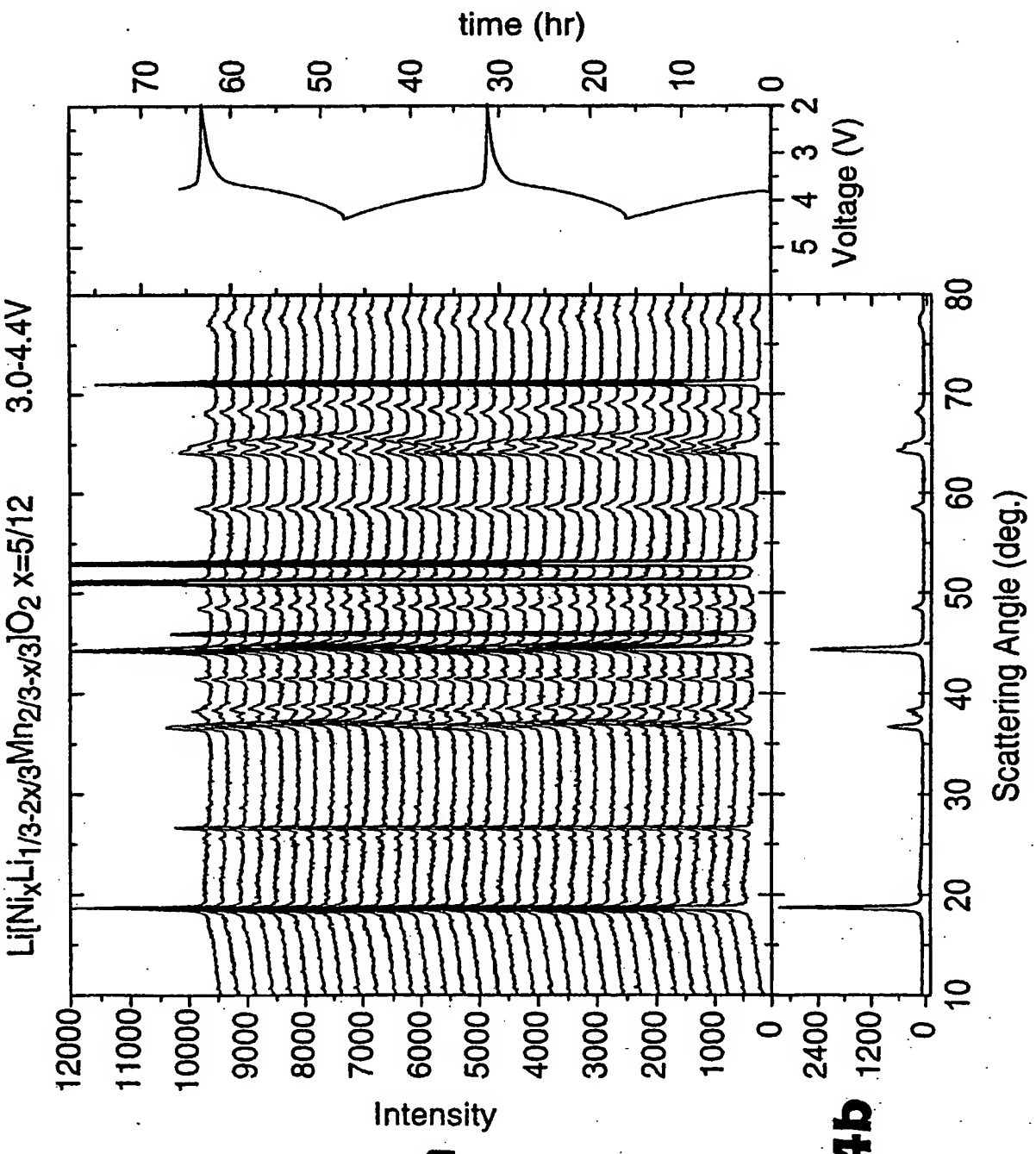

Fig. 4c

Fig. 4a

Fig. 4b

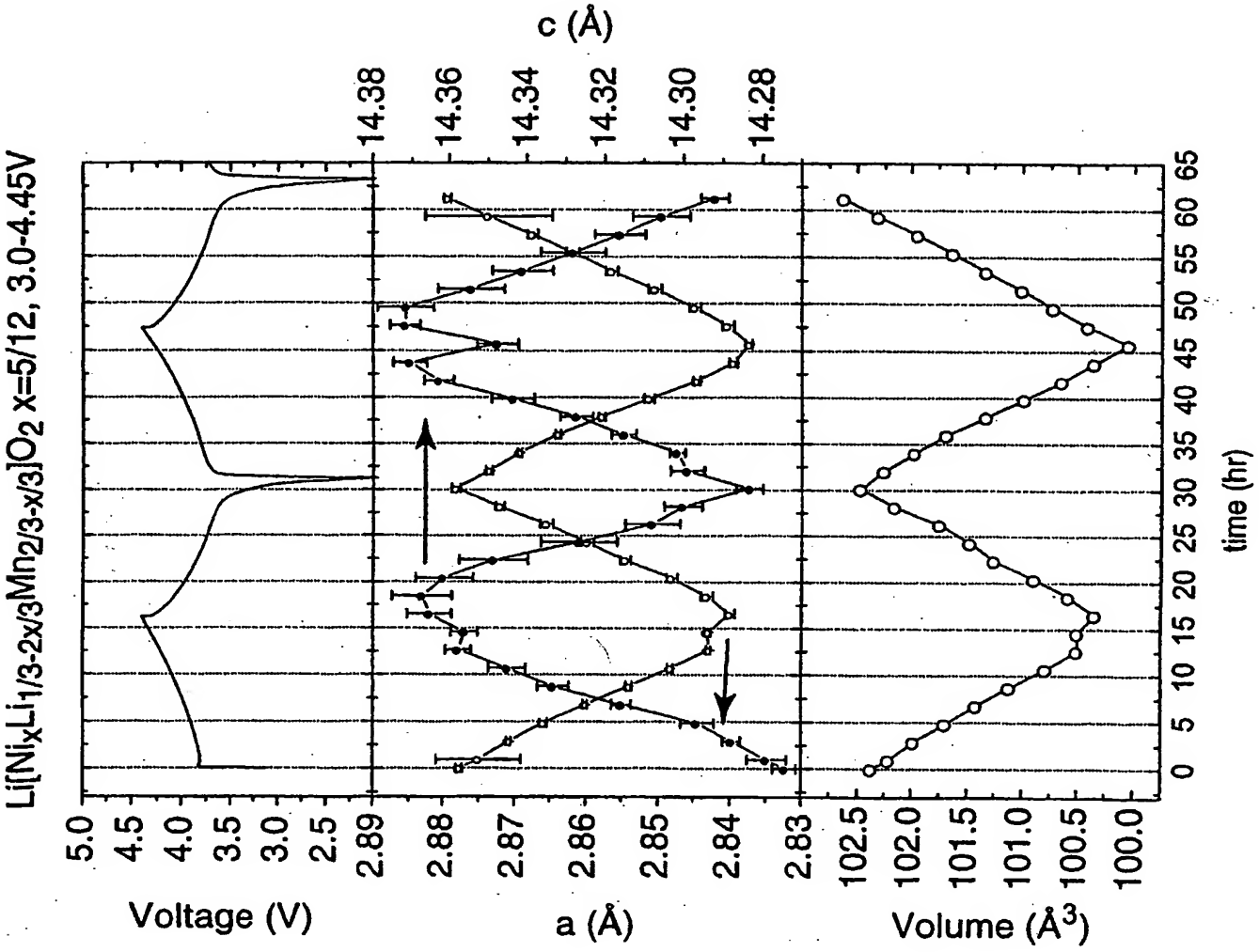

Fig. 5a

Fig. 5b

Fig. 5c

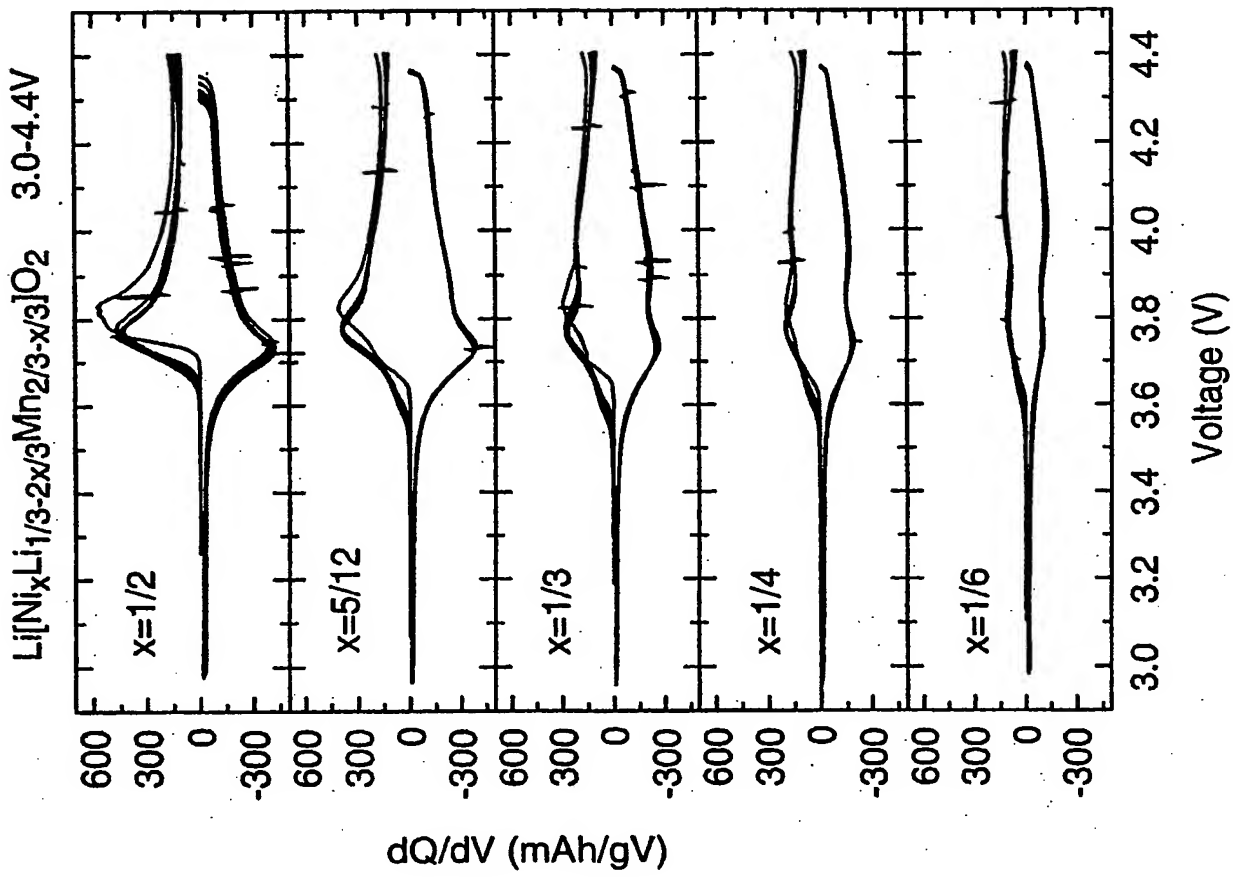

Fig. 6a

Fig. 6b

Fig. 6c

Fig. 6d

Fig. 6e

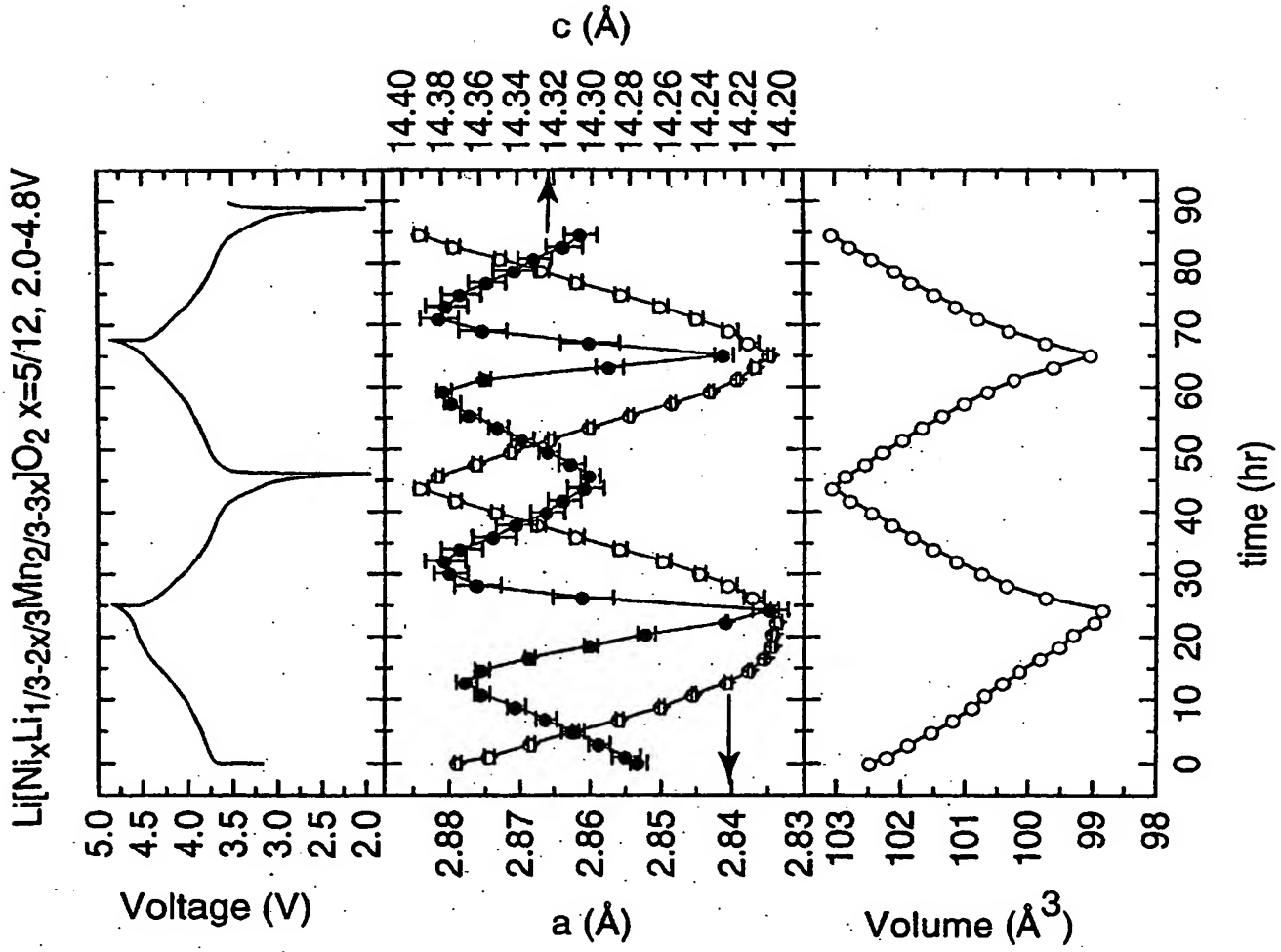

Fig. 7a

Fig. 7b

Fig. 7c

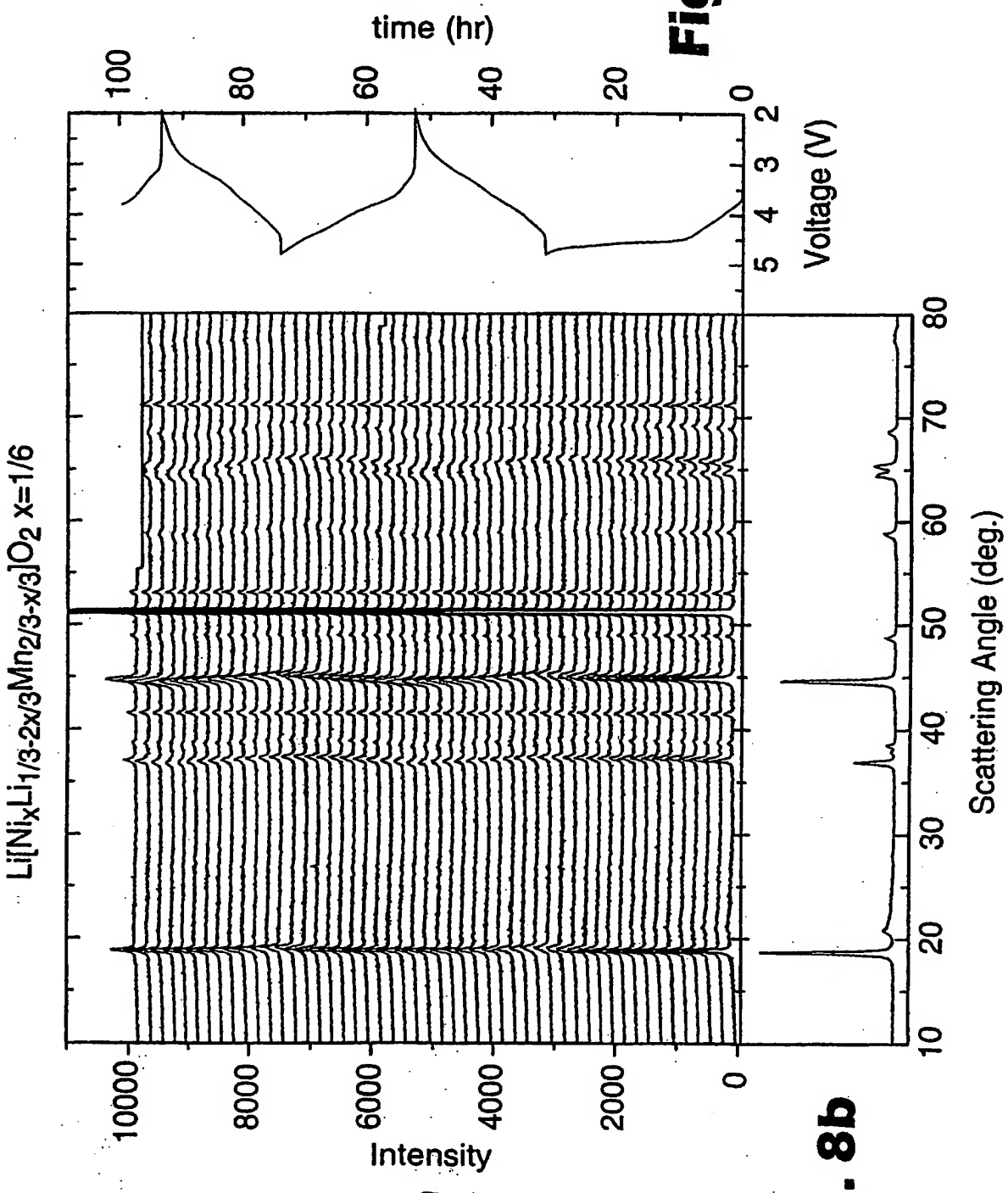

Fig. 8c

Fig. 8a

Fig. 8b

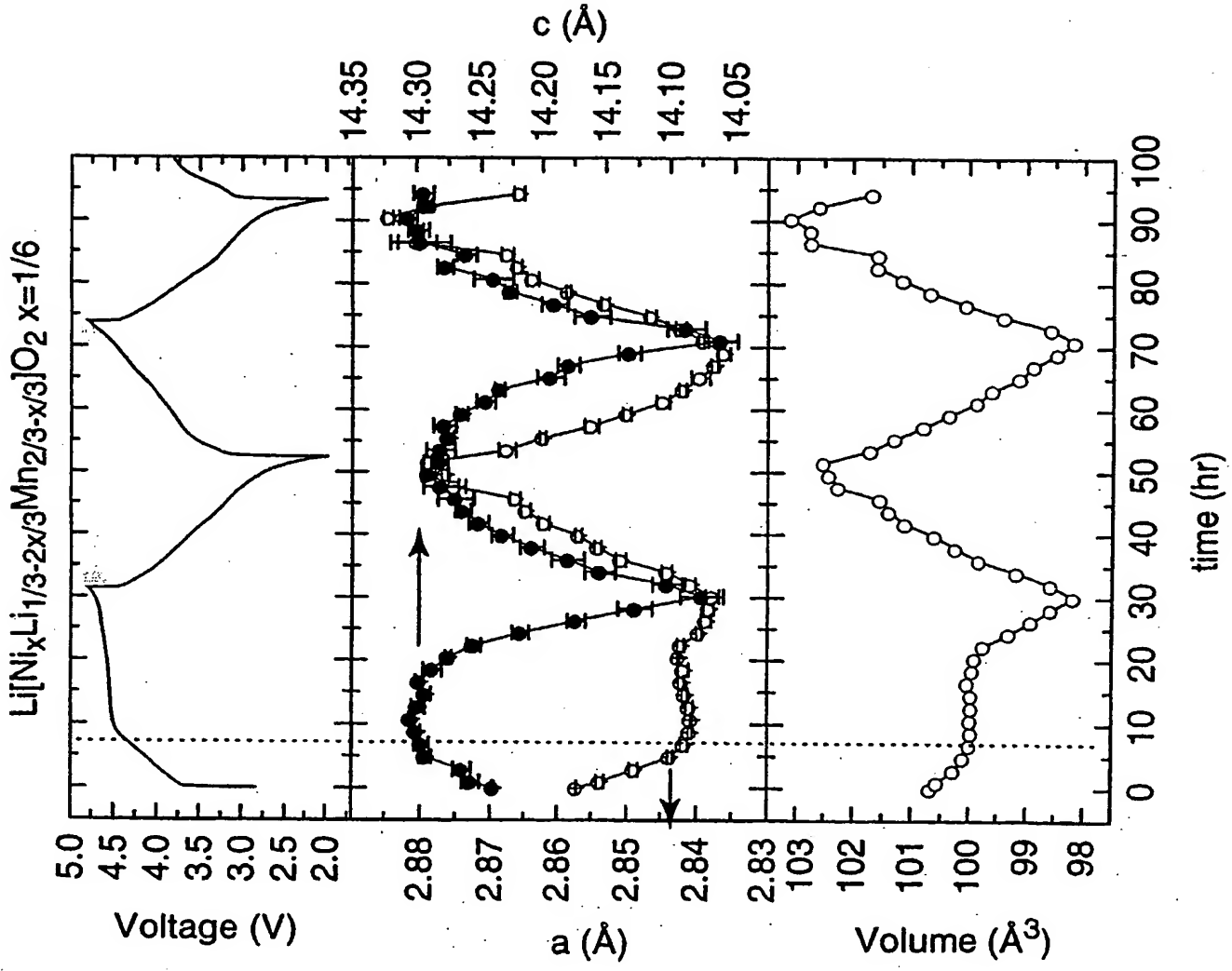

Fig. 9a

Fig. 9b

Fig. 9c

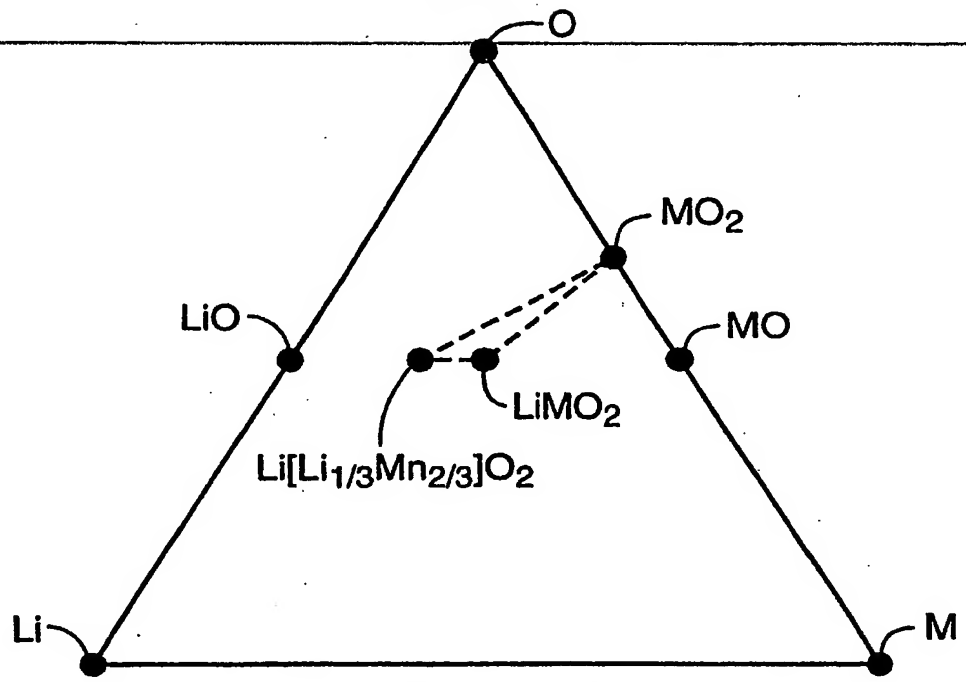
O
MO_2
LiO
MO
$LiMO_2$
$Li[Li_{1/3}Mn_{2/3}]O_2$
Li
M

Fig. 10

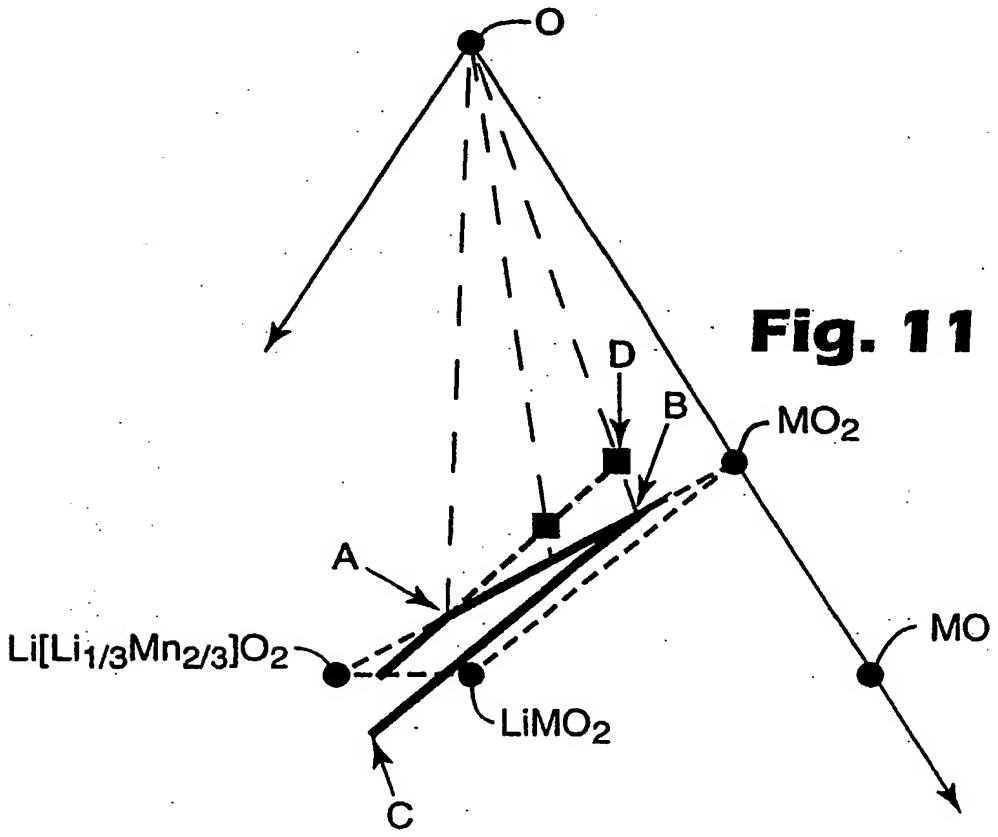
O
D
B
MO_2
A
$Li[Li_{1/3}Mn_{2/3}]O_2$
MO
$LiMO_2$
C

Fig. 11

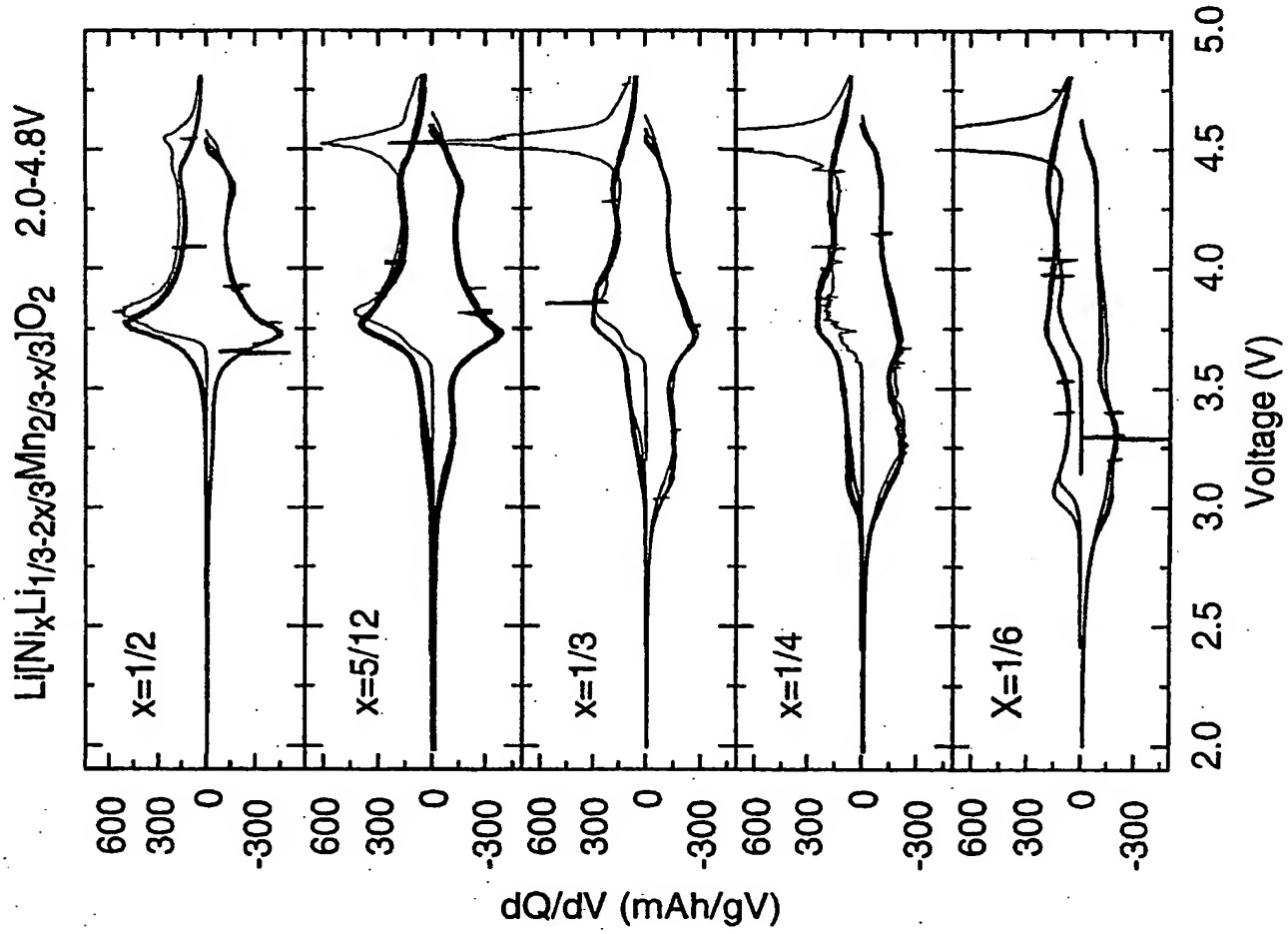

Fig. 12a

Fig. 12b

Fig. 12c

Fig. 12d

Fig. 12e

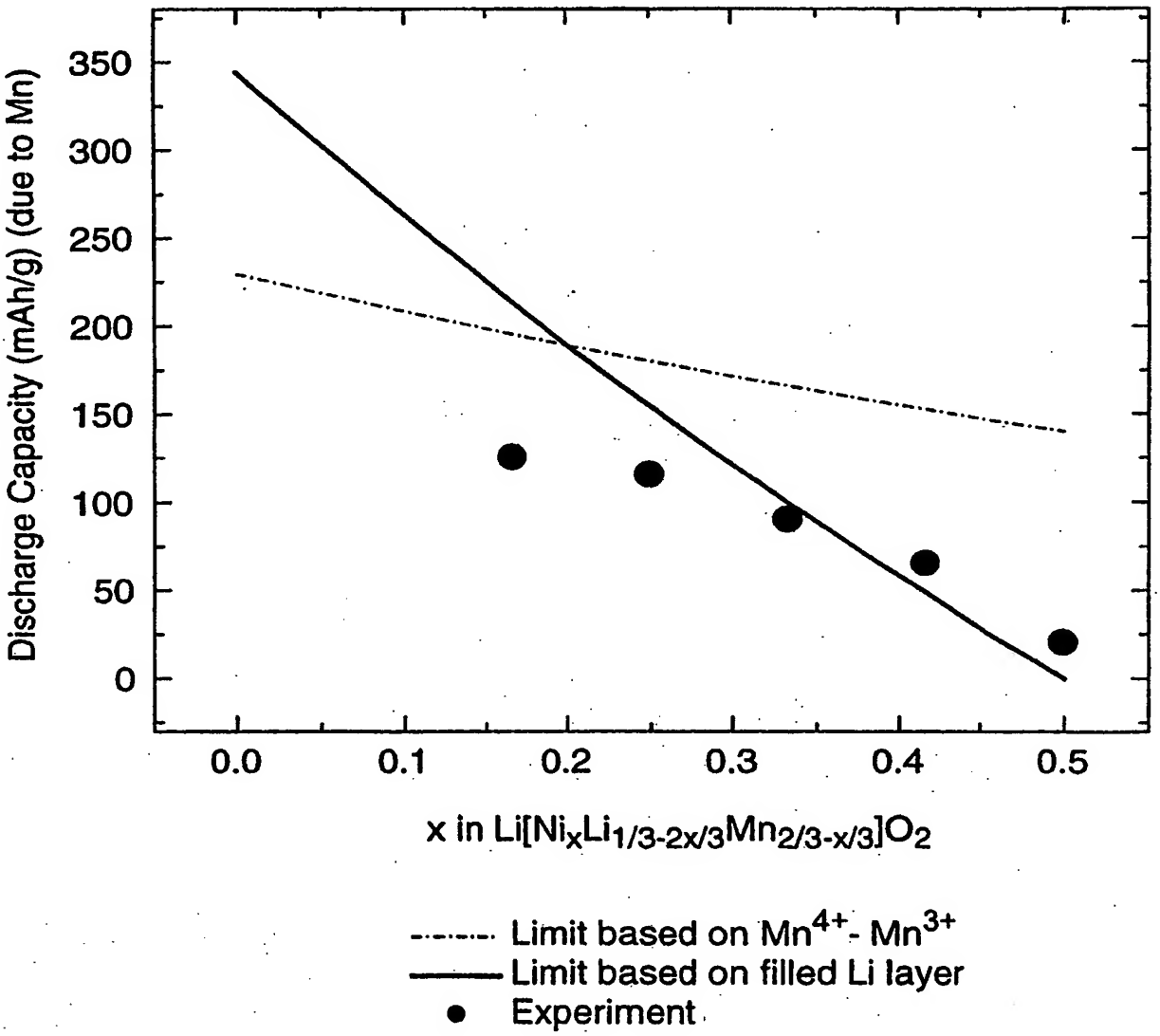
Discharge Capacity (mAh/g) (due to Mn)
350
300
250
200
150
100
50
0
0.0
0.1
0.2
0.3
0.4
0.5
x in Li[NixLi1/3-2x/3Mn2/3-x/3]O2
Limit based on Mn4+- Mn3+
Limit based on filled Li layer
Experiment

Fig. 13

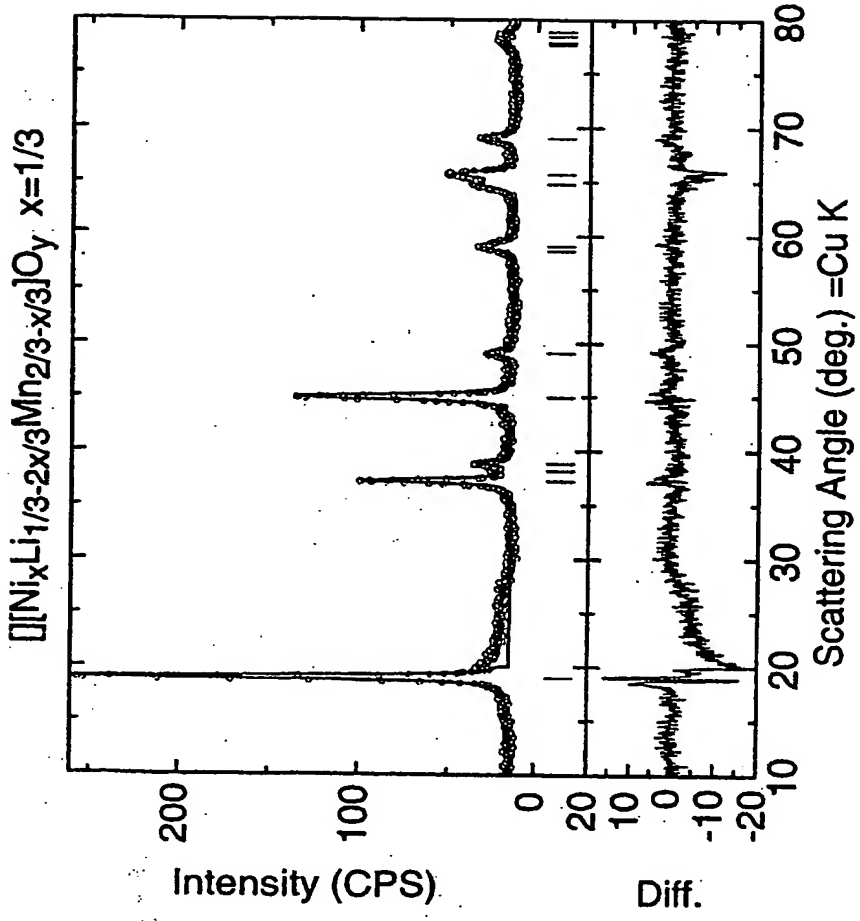

Fig. 14a

Fig. 14b

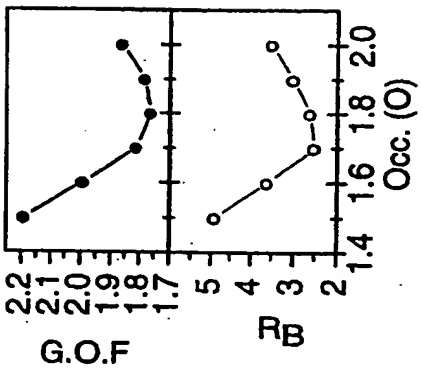

Fig. 14c

Fig. 14d

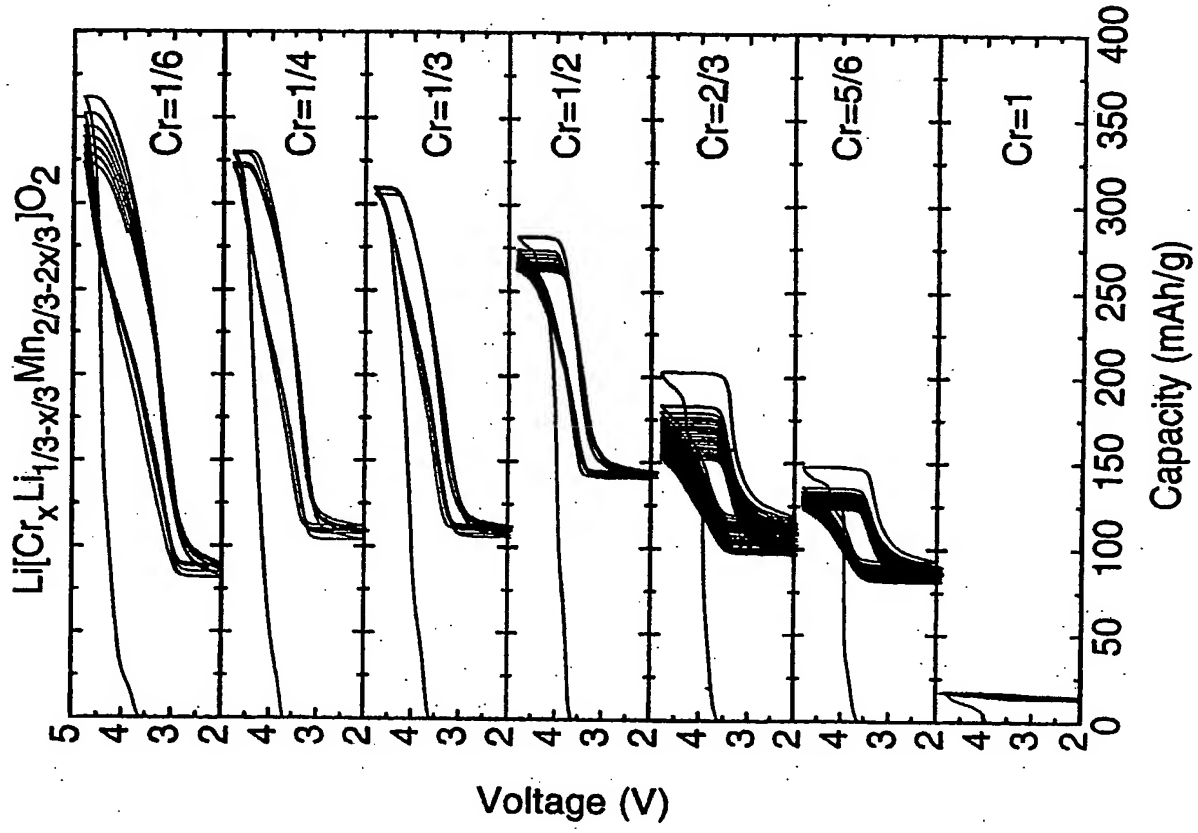

FIG. 15a

FIG. 15b

FIG. 15c

FIG. 15d

FIG. 15e

FIG. 15f

FIG. 15g

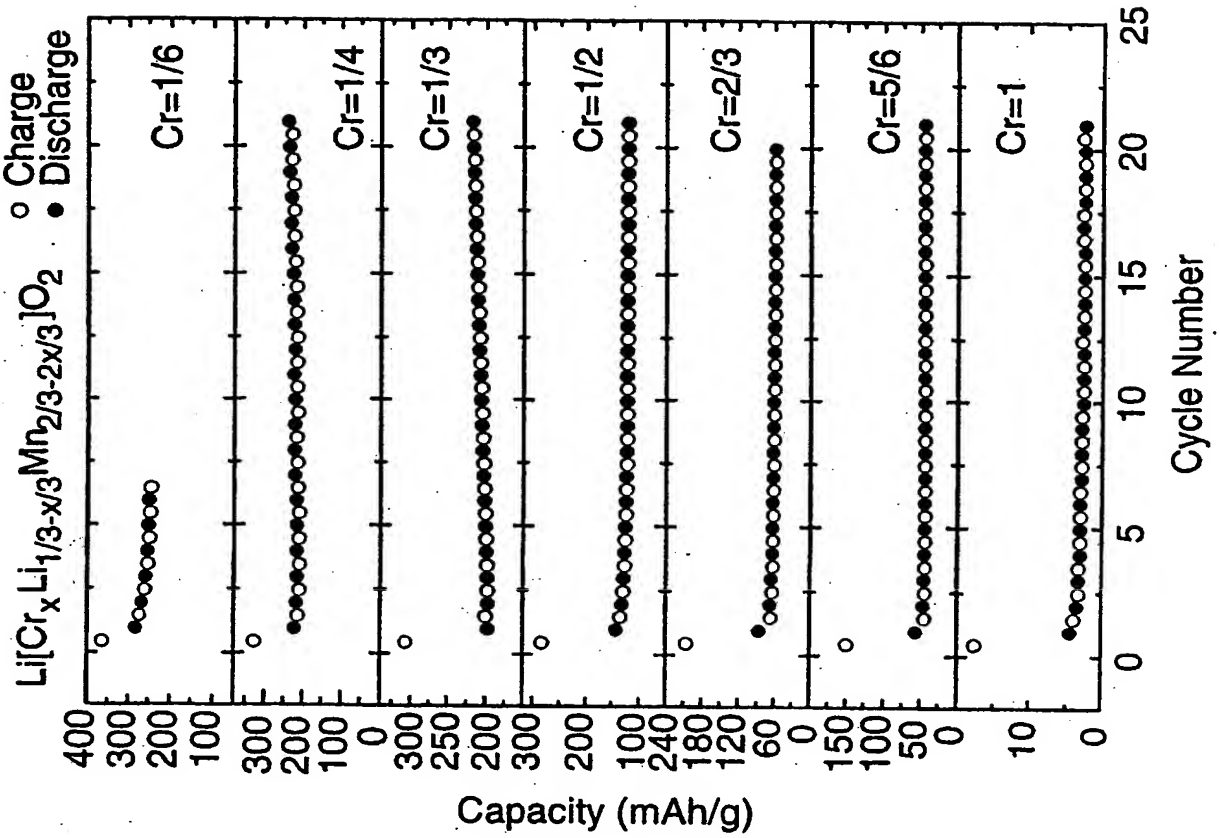

FIG. 16a

FIG. 16b

FIG. 16c

FIG. 16d

FIG. 16e

FIG. 16f

FIG. 16g

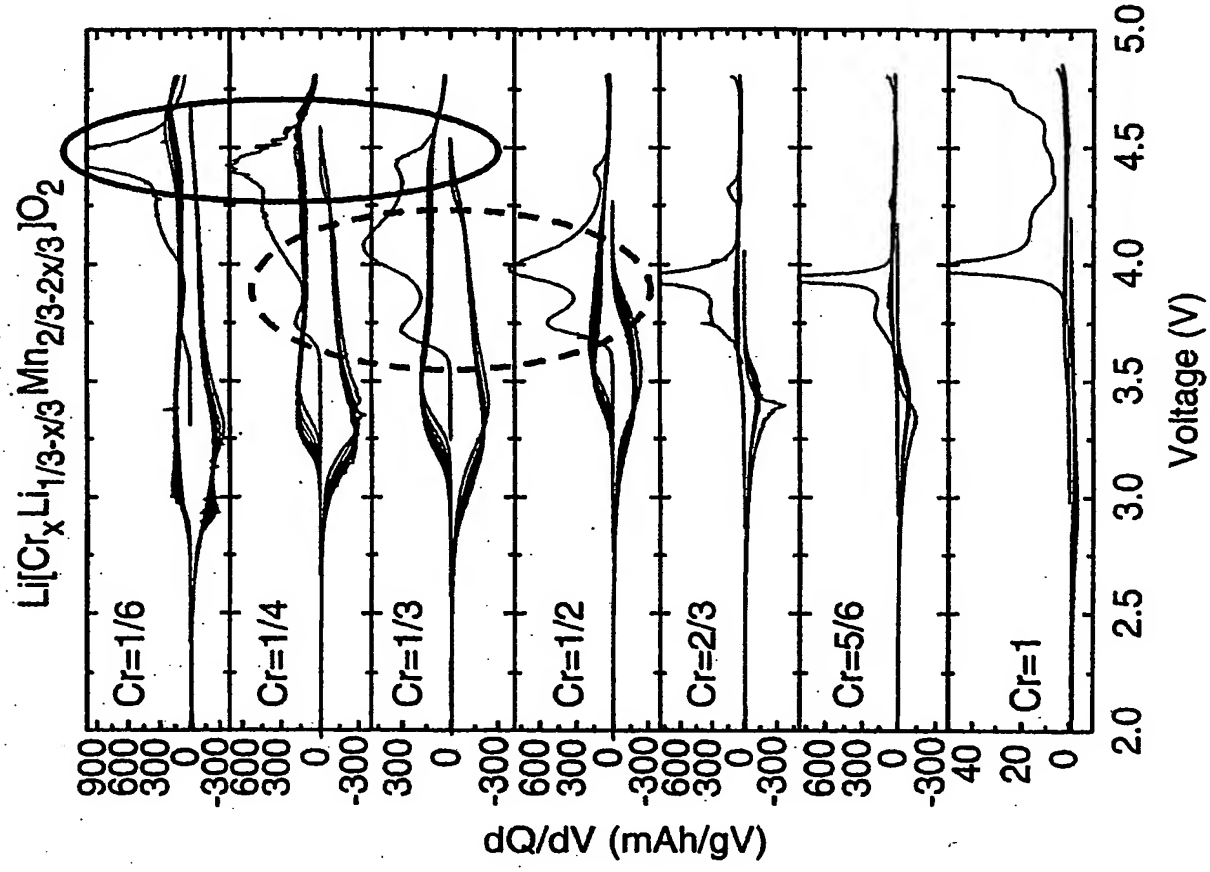

FIG. 17a

FIG. 17b

FIG. 17c

FIG. 17d

FIG. 17e

FIG. 17f

FIG. 17g